FAST NEUTRON

TOTAL CROSS SECTIONS

A Thesis

Submitted to

the Faculty of Graduate Studies and Research

of McGill University

in Partial Fulfilment

of the Requirements for the Degree

Doctor of Philosophy

by

Gerald Xavier Amey

July, 1964 Montreal, Quebec

SUMMARY

A transistorized, neutron time-of-flight spectrometer has been designed and built for measurement of the energy of neutrons generated with the aid of the McGill cyclotron. Circuitry of the type used in fast coincidence measurements has been used, with avalanche transistors as fast discriminators and limiters. The intrinsic electronic resolution is considerably better than one nanosecond.

The spectrometer was used to examine the radio frequency structure of proton pulses generated by the cyclotron. This was found to vary greatly with operating conditions and to depend greatly on the stability of the radio frequency oscillator. The short-term width at half height was 4 nanoseconds when the accelerating voltage applied to the dees was 7 kV, and the mean value of this quantity for long runs was 5-7 nanoseconds. With a flight path of 25 feet, the energies of neutrons or protons between 30 and 80 MeV can thus

be measured.

The total cross sections for neutrons of calcium, potassium and copper were measured in the range 30 to 100 MeV and found to confirm existing measurements except in the case of calcium. The deep minimum found at about 36 MeV by Moody was not confirmed, though energy resolution was sufficient to detect it.

ACKNOWLEDGEMENTS

The author wishes to thank Dr. R.E. Bell for suggesting this project and for much advice and guidance in designing the circuitry and interpreting the results.

The assistance of Mr. S. Doig and the workshop staff in designing and making mechanical parts, and of Mr. K. Heinstein in electronic matters is gratefully acknowledged.

Thanks are due to Dr. R.B. Moore, Mr. R.H. Mills and all those who aided in keeping the cyclotron operational, and to Mr. P. Portner whose Faraday cup became an essential part of the measurement system.

Genuine appreciation is expressed to the National Research Council for financial assistance throughout the extent of the work.

LIST OF FIGURES

TABLE OF CONTENTS

1. INTRODUCTION

For about a decade, nuclear physicists working in the 10 to 100 MeV region have made an intense study of the nucleon-nucleon interaction and have attempted to determine optical potentials which describe the interaction of a nucleon with a nucleus. In both cases a prime requirement is that the energies of the incoming and outgoing particles should be determined as accurately as possible. This is a relatively simple matter in the case of charged particles such as protons whose energy spectra may be accurately determined by some form of magnetic spectrometer, or by the height of pulses excited in a scintillator, or by degrading the energy in absorbing material.

None of these methods is available in the case of the neutron which otherwise would be the favoured particle for exploring the nucleus since the interaction potentials in this case are not complicated by the presence of a Coulomb term. Another difficulty associated with the neutron is that of obtaining a truly mono-

energetic beam of neutrons of high energy. As a consequence, experiments at energies above some tens of MeV must always be carried out with a more or less continuous spectrum of neutrons.

The usual method of generating high-energy neutrons involves the bombardment of a thick target with protons from an accelerator which, by its nature, produces particles in short bursts synchronized with a radio frequency field. This fact forms the basis of the time-of-flight method of measuring neutron energies.

For relativistic particles

$$\beta^2 = \frac{E^2 + 2m_oE}{E^2 + 2m_oE + m_o^2}$$

$$= \frac{2E}{2E + m_o} \qquad \text{to first order}$$

and since, for a flight path of length 'l', which is traversed in time 't':

$$\frac{dt}{t} = \frac{dE}{2E} - \frac{dE}{2E - m_o}$$

it is evident that energies may be determined with good resolution if the flight path is long and the particles

are not too relativistic. In the above formulae the symbols represent the following:

E kinetic energy (maximum 100 MeV with the McGill cyclotron)

m_o rest mass of the proton in MeV

t time of flight for a distance 'l' feet, measured in nanoseconds

β ratio of the velocity of the proton to that of light in free space

Since light travels one foot in one nanosecond (with an error of less than one percent) and $\beta = 0.43$ at about 100 MeV, a spectrometer with a resolving time of one nanosecond will give an energy resolution of 1% if the path length is 86 feet, if the proton always has the same phase with respect to the radio frequency field, on leaving the cyclotron. In fact the time structure of the proton burst in low-energy, fixed frequency cyclotrons is naturally of the order of about one nanosecond, so that excellent energy resolution can easily be obtained with such machines even with short flight paths (since the proton velocity is also much lower) In synchrocyclotrons protons may be accelerated

over as much as 120° of the radio frequency cycle because of the phase-stability characteristic (1) and consequently the time structure of a proton burst is correspondingly broadened. Under normal operating conditions (with 7.5 kV accelerating voltage on the dee) the breadth of this structure is about 5 nanoseconds at half peak height, in the case of the McGill cyclotron.

Low-energy proton bursts may be bunched by methods such as that first proposed by Mobley (2), however the electrostatic deflection involved is impractical in the case of high-energy protons and a high repetition rate. The time structure may be sharpened by lowering the cyclotron field or other changes which ensure that only those protons accelerated over a very small and fixed part of the radio frequency cycle may be extracted. By such means a two nanosecond proton pulse has been obtained with the McGill cyclotron, but operation was unstable, and phasing of the proton with respect to the radio frequency field sometimes changed sporadically. Of course, any such method inevitably decreases the proton flux drastically.

One advantage of a neutron source consisting of a

proton accelerator and a thick target lies in the production of a complete spectrum of energies extending almost up to the energy of the initial proton beam when an appropriate target is used.

The proton bursts, each about 5 nanoseconds wide, are emitted at 46 nanosecond intervals, for about 10 microseconds during each frequency modulation sweep, and there is no way of tagging which radio frequency cycle is associated with a given proton. Hence to avoid ambiguity as to energy, it is customary to deflect a single burst of protons on to the neutron generator once in each swing of frequency modulation. This automatically limits the maximum possible count rate to several hundred per second, and requires cluttering up the cyclotron cavity with deflection plates. The McGill cyclotron tank is already crowded and it was not considered desirable to make further additions for this purpose.

Alternatively, as in our case, the beam is not swept on to a target, the ambiguity being eliminated by restricting the range of the neutron spectrum being examined. This is easily achieved at the low end of the energy range, by biasing the scintillation detector so that only those recoil protons in the plastic, which have an energy greater

than the desired minimum will operate the system. For this purpose a transistor operating in the avalanche mode provides an excellent discriminator.

Control of the upper limit of the spectrum may be achieved by generating the neutrons within the cyclotron at the appropriate radius. In our case the available flight path in this case was too short so that it was decided to use the external beam. The only useful control of the upper energy limit of the spectrum is then provided by the choice of neutron generator, the nature of the reaction involved determining the maximum energy of neutrons emitted. Aluminum was used as it has a neutron peak at an energy of about 80 MeV. With a flight path of 25 feet it is then possible to cover a neutron energy range of 30 to 80 MeV without introducing ambiguity due to the overlap of the radio frequency structures of the high and low energy particles because of the periodic nature of the time scale. The time range is then 64 to 104 nanoseconds leaving the remaining 6 nanoseconds to provide for overlapping of flight times for low and high energy neutrons.

The energy resolution then varies from 10 to 15% over the energy range when the time structure of the proton burst

has a width at half-height of 5 nanoseconds, and is adequate for detecting the giant size resonances found in high-energy neutron cross sections which are of the order of 30 MeV wide. The most appropriate comparison is with the Harwell time-of-flight equipment in which the flight path is 27 metres and the half-width of the radio frequency structure 9 to 11 nanoseconds, their resolution thus being better by 27% at any energy. There is sufficient flux in our external beam to justify seeking a longer flight path and deflecting every second burst of external beam protons, as suggested by Dr Bell, so as to increase both the resolution and the spectral range that can be simultaneously analysed.

The time-of-flight spectrometer built was used to examine the radio frequency structure of the proton pulse from the cyclotron and to measure a number of neutron total cross sections which had previously been measured at only a few isolated points in their spectrum. Monoisotopic materials were used to simplify interpretation..

Neutron total cross sections at high energies have broad maxima which can be explained by considering the

nucleus as a sphere of nuclear matter which can be described by relatively simple potentials, as proposed by Bethe as far back as 1935 (3). The effect of reactions was introduced by including an imaginary part in the potential. The optical model was not developed very vigorously however until Barschall (4) pointed out in 1952 that the gross structure of the resonances as a function of energy was similar for al nuclides but that the mean cross section and locations of minima and maxima varied systematically with atomic number. Feshbach, Porter and Weisskopf in 1954 (5) put the theory on a sounder theoretical basis and interest in development of the optical model has steadily grown from that time, with experimentalists constantly providing more detailed data with which to fit the potentials proposed by theoreticians.

The systematics of the location of maxima and minima of the giant resonances can be put on an intuitively more satisfactory basis by considering their occurrence as due to a nuclear Ramsauer effect as was done by Peterson (6) following the suggestion of earlier authors. The nucleus is represented as a square well of radius R, and k_o and k_i are the wave numbers of neutrons outside and inside the well

well. In the absence of refraction, the average path length through a spherical nucleus is 4R/3. The average phase difference for waves passing through and around the nucleus is

$$\frac{4}{3}\ (k_i - k_o)R \qquad n$$

where is a constant which corrects for the refraction effect. Maxima occur when there is destructive interference between the two wave components, that is, when

$$-\quad 0, \text{ that is when } n \quad 1,3,5,...$$

and minima when 'n' is even. The connection with optical well theory lies in the selection of an energy-dependent potential for the determination of the value of k_i for the neutron inside the nucleus. Peterson extrapolated the data of Bjorklund and Fernbach (7) using the energy dependence calculated by Riesenfeld and Watson (8).

Despite the simplicity of the theory, agreement with experiment is quite good, the locations of maxima and minima being predicted with fair accuracy when account is taken of the fact that this Ramsauer oscillation in total cross section is to be added to the monotonically decreasing curve derived from the black-nucleus model, known to

give the correct average cross section.

Amongst the cross sections measured was that of calcium, which had been previously been investigated at this laboratory (11), a much sharper resonance being found by Moody than that to be expected from theory and the results obtained for other elements. The breadth of this resonance at half-maximum was said to be 8 MeV and its centre energy 37 MeV. The resolution of the present equipment was adequate to determine the existence or nonexistence of this resonance.

2. DISCUSSION OF THE EXPERIMENT

2.1 Theory

Total cross sections are obtained by placing an attenuator in the path of a stream of neutrons and finding what proportion of the neutrons passes undeflected and unabsorbed through the absorber. When care is taken great accuracy can be attained and the information is of considerable value to theoreticians. Since only comparative flux measurements need be made it is not necessary to know the absolute efficiency of the counter employed.

The sample is so placed as completely to shadow the neutron source. When dealing with low energy neutrons from a sharply defined source, normally no shielding is used for the detector. All installations built for investigating high energy neutrons use massive shielding and collimation, principally because the neutrons are generated from protons accelerated in cyclotrons which provide a continuous, diffuse (in space and time)source of fast neutrons apart from those specifically produced in the neutron generator. In the present case, as an external beam was used which contained only 2% of the

protons accelerated to 100 MeV, the shielding problem is evidently exaggerated, as approximately fifty times as many neutrons will be produced at the regenerator used for extracting protons as in the neutron generator itself.

The relative flux decrease in a sample of thickness 'dx' is:

$$dI/I = -n\sigma dx \qquad (1)$$

where 'n' is the number of nuclei per cm^2 of the sample, 'I' the flux in neutrons/cm^2sec and σ the total cross section. Integrating eqn. (1) from 0 to 't' the total sample thickness, we obtain:

$$I = I_o e^{-nt\sigma} \qquad (2)$$

The experimental procedure then simply consists in measuring flux at the detector with the sample in (I) and out (I_o) thereby obtaining the transmission $T = I/I_o$. Hence the cross section is:

$$\sigma = \frac{1}{nt} \ln \frac{1}{T} \qquad (3)$$

Apart from corrections for background, deadtime of counters etc, the above equations do not take account of inscatter, that is, correction for scattering in the 0^o direction, nor of the hardening effect which may

arise when the cross section varies greatly over the energy range of neutrons and which causes the total flux attenuation to be non-exponential.

2.2 Experimental Layout

A long flight path is essential if good energy resolution is to be achieved, but the layout had to be a compromise between this requirement and the geometry of the existing space. For this reason, and because of shielding difficulties it was decided not to use the internal beam. Use of the latter would give flexibility in regard to the choice of the upper energy of neutrons to be generated, as well as a flux fifty times that of the external beam. In our case the flux available from the external beam appeared adequate as the method used ensured efficient utilisation of the available protons. We were not really interested in doing work below 30 MeV as this region has been covered fairly thoroughly and background problems are much more severe when it is desired to detect particles at energies below this value. Hence a continuous spectrum generated from a 100 MeV proton source was ideal for our purposes. The remaining option, once we have available the

spatial flexibility given by use of the external beam, was as between the shielded corner of the cyclotron vault near the 30° magnet (see Fig. 1) and location in the beam hall.

Use of the beam hall would allow a flight path twice as long as that available in the vault and hence 40% better energy resolution. As many other experiments were planned for this room, which furthermore was incomplete when this experiment was commenced, it was decided to use the vault location, despite the high background and the shorter flight path. Neutrons are generated at the neutron generator, pass through a window in the shielding, between the poles of the 30° bending magnet, which was initially used to sweep aside protons resulting from energy degradation in the neutron generator, and thence via a one inch collimator to the shielded scintillation detector, M.D. The monitor, Mon, is a similar detector situated a few degrees away from the main detector and seeing substantially the same neturons. The flight path is 25 feet, thus allowing an energy resolution of 10% at 30 MeV when the time resolution is 5 nanoseconds. The solid angle is then about

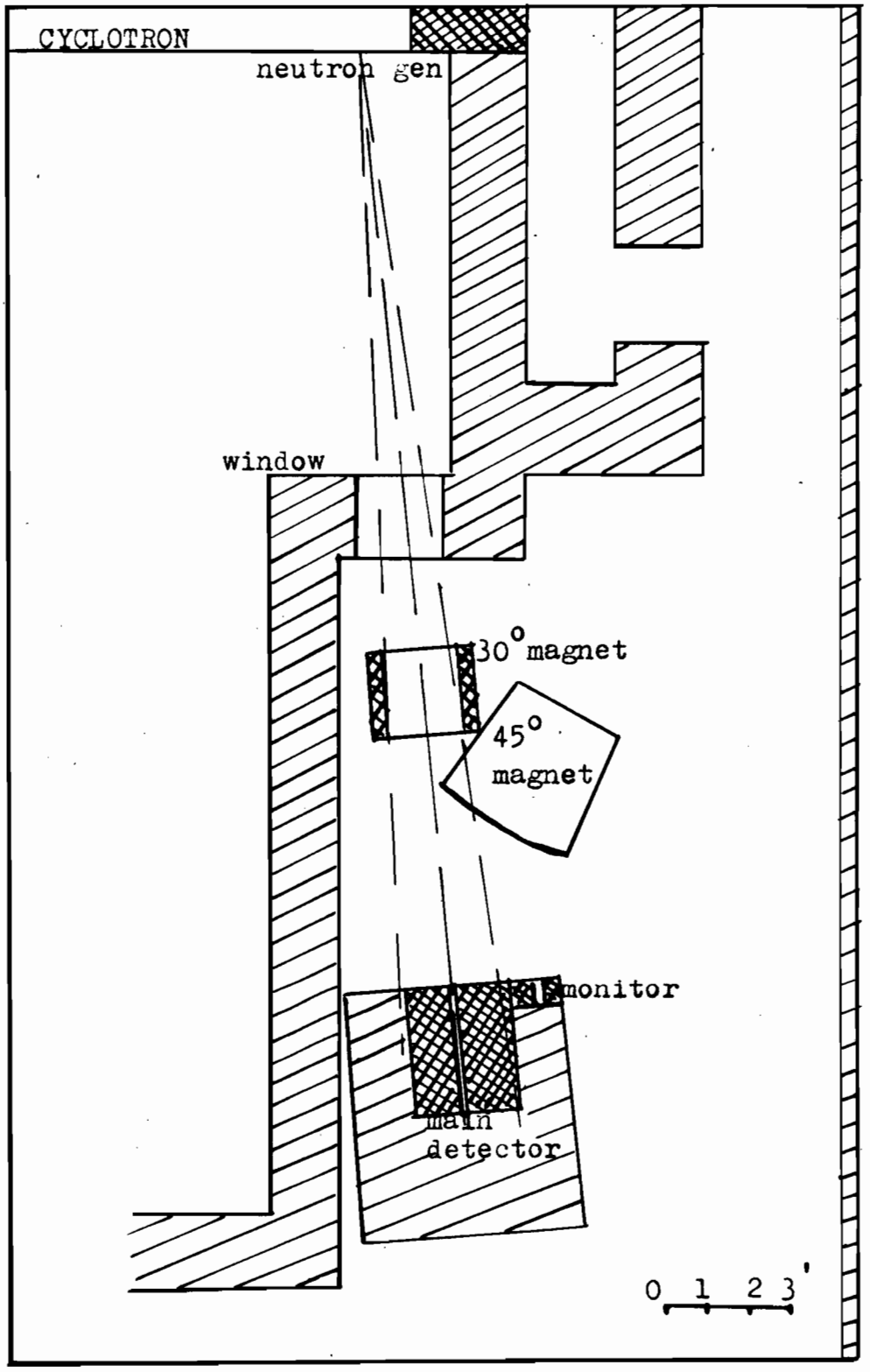
CYCLOTRON
neutron gen
window
30° magnet
45° magnet
monitor
main detector
0 1 2 3'

FIG 1

10^{-5} steradians. The details of this arrangement had to be modified subsequently as is explained in the chapter devoted to the actual experiment, the solid angle thereby being reduced to 10^{-6} steradians.

If we use the figure of Hofmann et al. (12) of 2.6 millibarn/steradian-MeV for neutron production by an aluminum target, and a proton current of 3×10^{10} per second, we would expect a neutron flux from a 1¼ inch target into the energy range, 30-100 MeV, of about 390 per second into 10^{-6} steradians. When a plastic scintillator 4 inch long is used as the detector, an efficiency between 15 and 20% can be expected in this range according to Wiegand et al (10), hence the raw counting rate should be 45 per second, when attenuation by the ¾-inch thick brass Faraday cup is taken into account. This ignores nuclear attenuation of the beam in the aluminum target itself, and the fact that the cross section decreases with energy. The small bore collimator was aligned with the center of the beam tube by placing a lamp at this point and looking directly through the small bore and the one-inch diameter collimators. The fact that the proton beam, as seen in Fig. 2 is not centered on this point, and that alignment of the collimator was not perfect gave rise to a lower flux. The raw counting

rate was actually about 16 per second, and adding thickness to the neutron generator did not seem to add appreciably to the neutron production at low energies in the 0^{o} direction. The same effect is seen in the work done at Harwell and elsewhere, but they do not discuss the matter. In order to improve the count rate it would be necessary to increase the solid angle subtended by the detector, and for reasons discussed later this would require that the collimator be placed much closer to the neutron generator than is possible with the present location. A factor of ten could easily be achieved by this means.

2.3 Neutron Generator

In Fig. 2, the arrangement of the neutron generators is shown. Provision is made for a choice of two targets, the dimensions of which must be such that they can be withdrawn into the side-arms having 2 inch internal diameter. The target mainly used was of aluminum, 70 MeV thick and 1½ inch square, mounted on a one-inch diameter rod. It later appeared that this did not completely cover the proton beam and additional collimation was required to eliminate effects due to neutrons generated between this point and

the detector due to protons not intercepted by the neutron generator but by obstructions in the beam tube.

2.4 Block Diagram (Fig. 3)

A marker pulse formed from the radio frequency signal picked capacitatively from the dee, is gated by a signal from Q_1, an avalanch transistor acting as a discriminator to accept pulses due to recoil protons of energy greater than 25 MeV, generated by neutrons in the plastic scintillator of the main detector. A step pulse, 60 nanoseconds long is also derived from Q_1 and added to a similar pulse derived from Q_2 which is triggered by the gated marker pulse. The sum pulse is used to charge a condenser from a constant current source in a time-to-amplitude converter of the type developed by Bell (9). After shaping and amplification, a signal of height proportional to the neutron time of flight is gated by a pulse from a dynode of the main detector, so that only pulses due to recoil protons with energies in a window from 30 to 40 MeV are accepted, and fed to the kicksorter. This is the classic fast-slow coincidence method originated by Bell (9).

In measuring a total cross section, a time of flight

spectrum is obtained for a number of counts registered by the monitor with and without insertion into the beam of the material being investigated. The signal from the monitor, which has a two-inch long plastic scintillator, passes to avalanche Q_6 (40 nanoseconds dead time), which acts as a discriminator to ensure that only neutrons of similar energy to those detected by the main crystal, are counted by the scaler which has one microsecond time resolution, after gating by the dead-time gate. The latter is controlled by a signal 15 microseconds long, derived by means of a univibrator from an output of Q_1 and ensures that monitor pulses are not counted during the dead time of the main time analyser. The much longer dead time of the kicksorter need not be taken into account separately as the entire proton burst is only 10 microsecond long and thus shorter than the dead time of the time- analysing circuits. As the scaler has a resolution of one microsecond, its maximum counting rate is 4,000 per second. The actual count rate was very much lower than this so that the counting error was negligible.

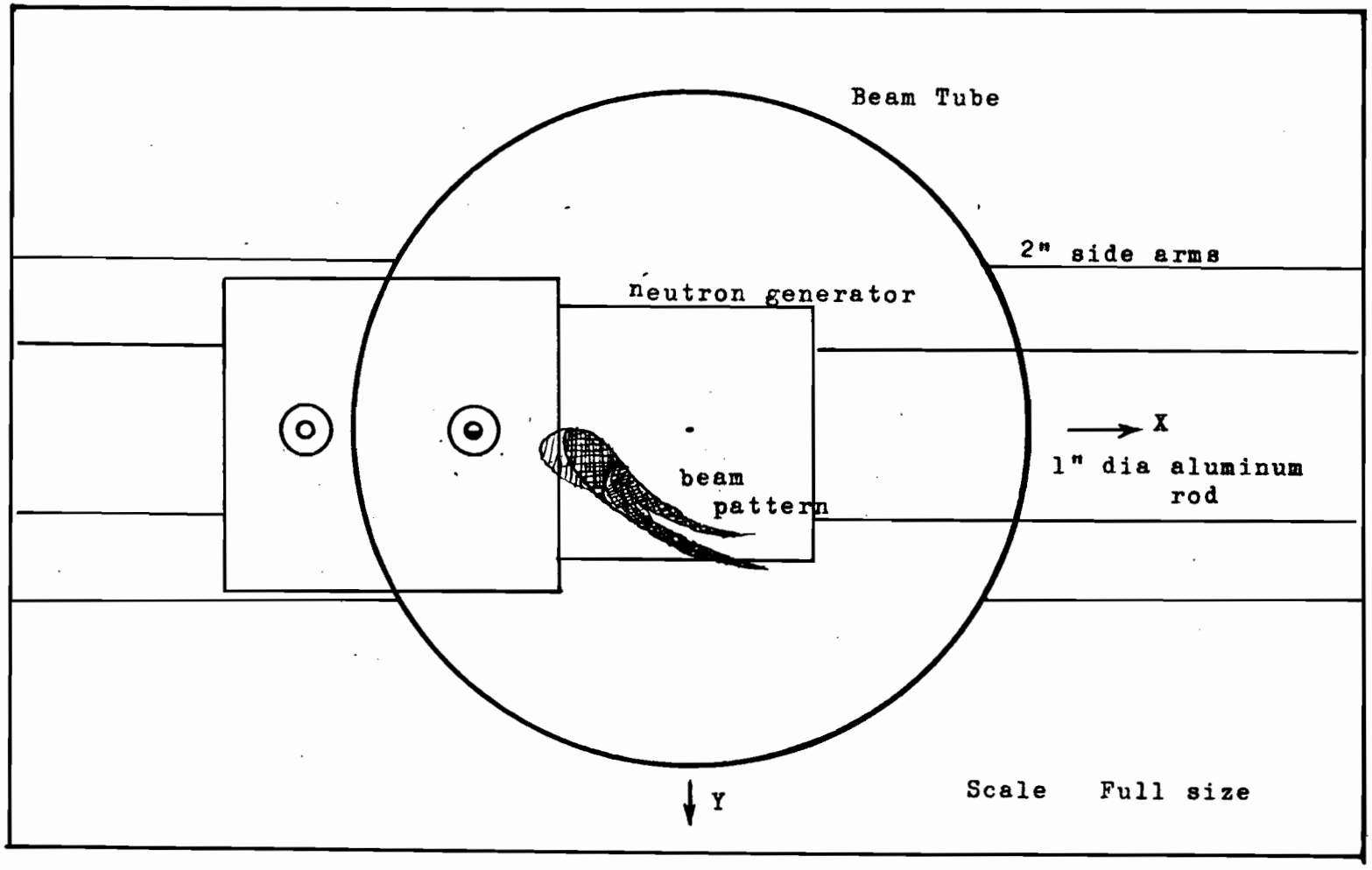
Beam Tube
2" side arms
neutron generator
X
1" dia aluminum rod
beam pattern
Y
Scale Full size

FIG 2

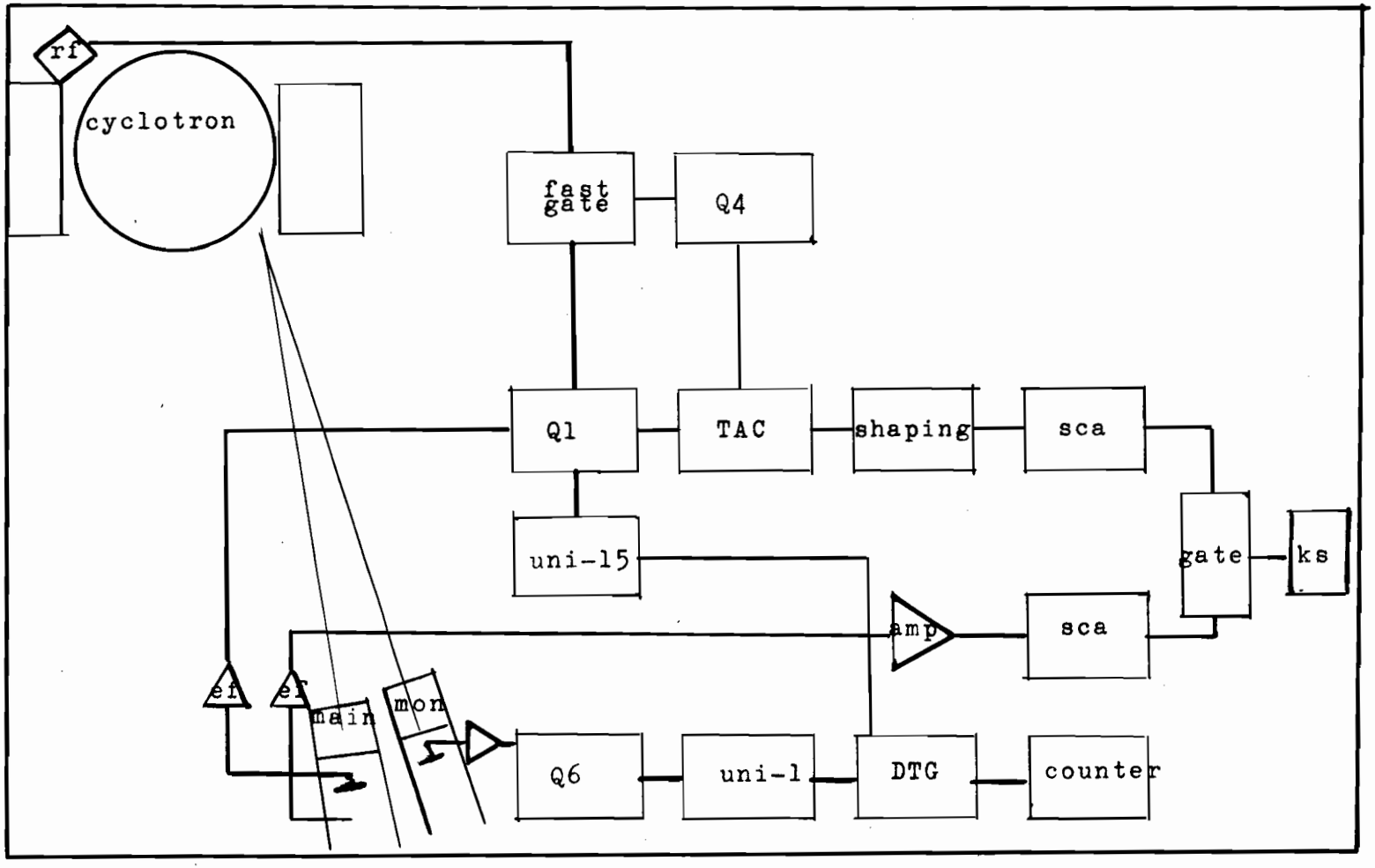
rf
cyclotron
fast gate
Q4
Q1
TAC
shaping
sca
uni-15
gate
ks
amp
sca
ef
ef
main
mon
Q6
uni-1
DTG
counter

FIG 3

2.5 Collimation and Shielding

The total neutron cross section for light materials such as those contained in concrete, is about 2 barns in the energy range, 20 MeV to 100 MeV, and about one-half the total cross section is due to elastic scattering and strongly peaked forward. The non-elastic part (mostly inelastic at high energies) is less strongly peaked in the forward direction. Hence if we consider a neutron to be effectively removed from the beam if it is scattered non-elastically, then after each mean free path, 65% of the particles will have been scattered, and about half of these, elastically. Thus only about one-third of the neutrons will be removed from the beam for each mean free path. Then, ignoring the slight degradation of energy and broadening of the beam due to elastic scattering, the beam will have $(2/3)^n$ of its initial intensity after 'n' mean free paths. To attenuate to 1% would require about 40 inch of concrete or 40 cm of iron.

Fig. 1 showed a plan of the equipment with reference to the shielding problem and Fig. 4 shows a side view. There are effectively two sources of high energy neutrons,

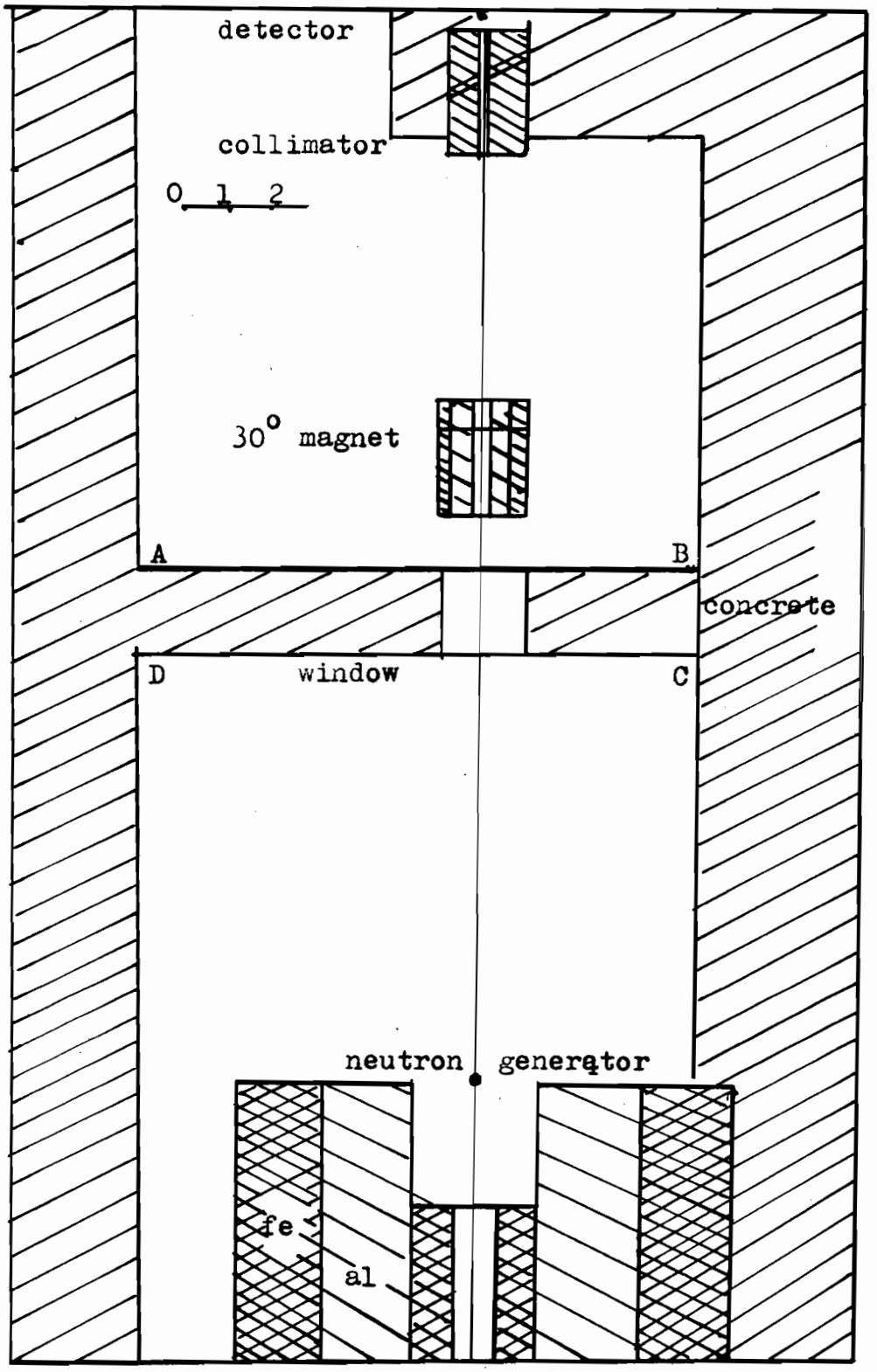
detector
collimator
0 1 2
30° magnet
A
B
concrete
D
window
C
neutron generator
fe
al

FIG 4

the neutron generator itself and the regenerator, which sees a flux of 100 MeV protons forty nine times as great as that incident on the neutron generator. Since the angle of separation of these two sources is small at the main neutron detector, the traditional method of measuring cross sections, in which only the absorber being measured is placed between source and detector, no collimation being used, is impractical. The existing shielding consisted of a two-foot thick concrete wall, extending from floor to ceiling, but having a window about two feet square at beam height, and some shielding supplied by the iron yoke and aluminum windings of the 30° bending magnet.

It was decided to use the shadow cast by this magnet as part of the required collimation, an iron collimator three feet long and pierced by a hole of one inch diameter, filling the region unshadowed by the magnet yoke. Additional shielding for neutrons not within a few degrees of the forward direction was provided by concrete blocks stacked to a depth of at least two feet in each direction. The shielding problem was simplified in this experiment by the fact that it was necessary to shield the equipment only from

neutrons possessing energies greater than about 25 MeV, the lower limit selected for the energy spectrum. When an infinite attenuator (a 42 inch iron rod) was inserted into the collimator aperture, the background counts remaining were found to be a negligible proportion of the counts when the hole was unobstructed. It was later found necessary to add an additional collimator, 4 inch in diameter, 18 inch long and pierced by a hole 23/64 inch in diameter, to eliminate spurious neutron generation by obstacles inserted in the neutron path by other experimenters after the present work was commenced.

2.6 Neutron Detector

The most efficient detector of high energy neutrons is a plastic scintillator used in conjunction with a photomultiplier. The neutrons give rise to recoil protons by collision with hydrogen atoms which form about 50% of the plastic. The protons then give rise to scintillations having a fast decay time and thus suitable for timing circuits of high resolution. Since the energy communicated to the proton can be any fraction of the energy of the original neutron, the height of the pulses at the photomultiplier output gives only limited information as to the energy of the neutrons incident on the crystal. Obviously the recoil

proton cannot have a greater energy than that of the neutron giving rise to it, and this fact is utilized to discriminate against low energy neutrons.

Fig. 5d shows schematically the apparent spectral distribution to be expected when detection threshold, efficiency and nature and thickness of the neutron generator are taken into account. Fig. 5a shows in idealized form the recoil spectrum arising from monoenergetic neutrons. Fig.5b is taken from a paper by Wiegand (10) devoted to a study of the efficiency of plastic scintillators as neutron detectors.

In the non-relativistic approximation, and assuming isotropic scattering we may take the efficiency of a plastic scintillation detector to be

$$\eta = \sigma nh \left(1 - \frac{B}{E}\right)$$

where E is the energy of the neutron, B the threshold bias of the detecting circuit, 'n' the number of hydrogen atoms per unit volume of scintillator, σ the total cross section for n,p- scattering, and 'h' the thickness of the scintillator. Absolute measurements of flux are not required in measuring neutron total cross sections, hence the relativistic correction and that for non-isotropic scattering can

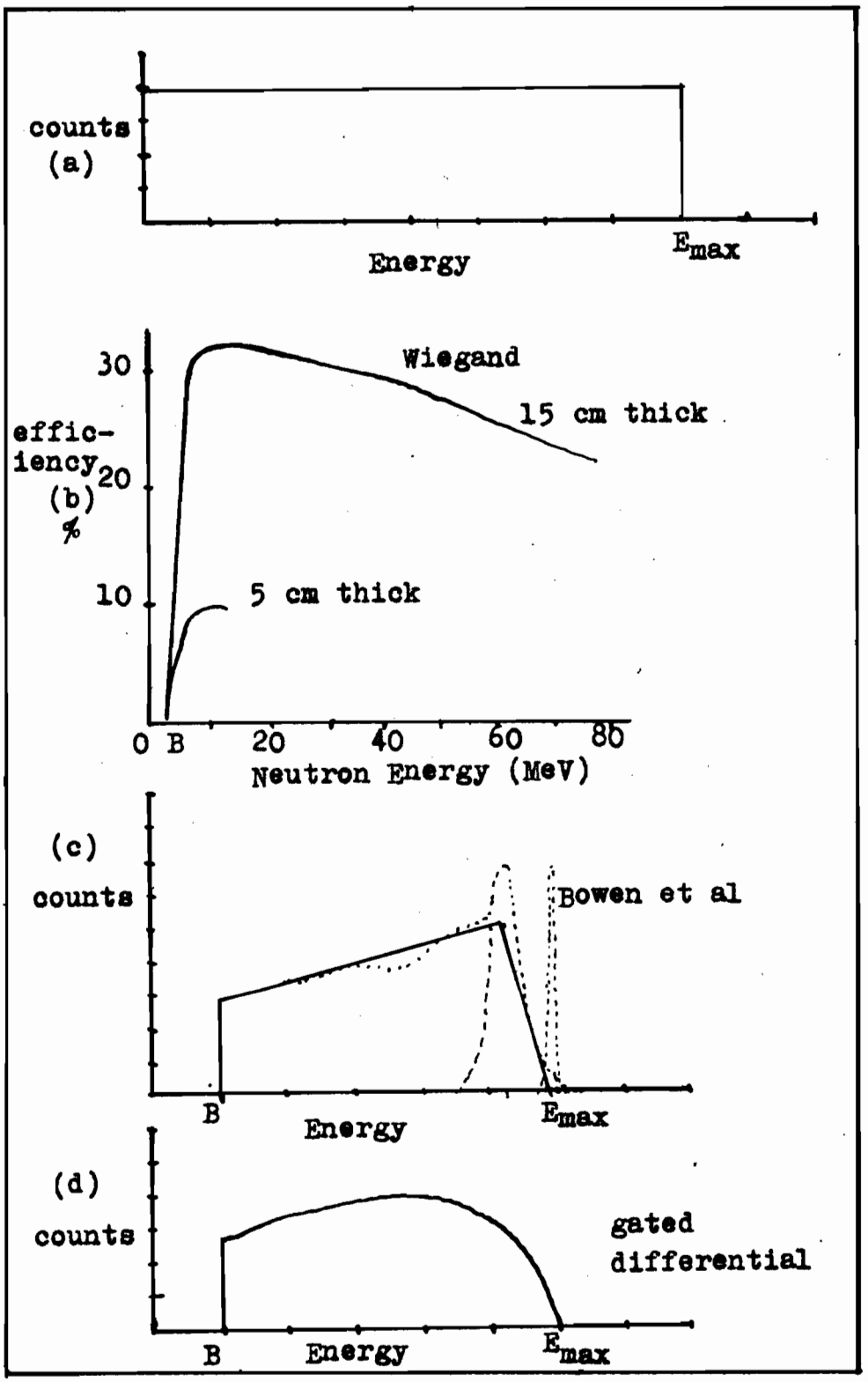
counts
(a)
Energy
E_{max}
30
20
10
effic-
iency
(b)
%
Wiegand
15 cm thick
5 cm thick
0 B 20 40 60 80
Neutron Energy (MeV)
(c)
counts
Bowen et al
B
Energy
E_{max}
(d)
counts
gated
differential
B
Energy
E_{max}

FIG 5

be ignored.

Fig. 5c shows schematically the energy spectrum of neutrons from a thick aluminum neutron generator. This is similar to those obtained in the present experiment and in experiments by Bowen et al. (15) in time-of-flight measurements. In the earlier work of Hoffman and Strauch, there appeared to be a much greater production of low-energy neutrons, but this may be due to the fact that their solid angle for detection was much greater than ours.

The application of a window in the slow part of the fast-slow analysis results in a further lowering of detection efficiency for neutrons of energy higher than the upper detection energy, E_m, only $\frac{E_m - B}{E - B}$ being detected. Therefore the efficiency of counting such neutrons is

$$\eta = \sigma n h \frac{E_m - B}{E}$$

The curves actually obtained in the present case are shown in the experimental section.

2.7 Resolution

It was shown in chapter 1 that the energy resolution of time-of-flight equipment is approximately twice as bad as the time resolution, which is made up of the following

Components:

2.7.1 time structure of the proton pulse

2.7.2 radio frequency pickup by the neutron detectors

2.7.3 time spread due to varying height of neutron detection pulses

2.7.4 electronic resolution and miscellaneous radio frequency pickup

2.7.1 Time structure of the Proton Pulse

The major contribution to the time resolution is that due to the time structure of the proton bursts generated by the synchrocyclotron. Because of the phase-stability characteristic of such machines, protons may be accelerated for about 1/3 of the radio frequency cycle which has a period of about 46 nanoseconds as the proton leaves the machine. When magnetic field and accelerating voltage were optimized to produce maximum external beam current, the half-width of this time structure was found to be 5 nanoseconds in the McGill cyclotron. When the accelerating voltage was reduced to 4.5 kV, the width of the burst was narrowed to 2 nanoseconds but operation was

unstable, this instability showing up as a short-term variability of the phase of the protons with respect to the radio frequency field. It is presumed that the oscillator can be made to operate stably at reduced voltages by suitable design modifications. Owing to additions to the building and other circumstances, very little time was available during the present investigation for studying the properties of the oscillator. The full potentialities of time-of-flight measurements will not be achieved until such work has been carried out.

Due to the width of the time structure of proton bursts, the other contributions discussed below, do not at present add notably to the resolution.

2.7.2 Radio Frequency Pickup by Neutron Detectors.

The 30 kw oscillator which provides the proton-accelerating field is at present quite inadequately shielded. Despite the use of complete shielding for the detectors, the pickup at the input to the main discriminator was sometimes as much as a half volt peak-to-peak. As shown in Fig. 6a, if the avalanche discriminator is biassed to trigger on 5V pulses, and the neutron pulse has a risetime from

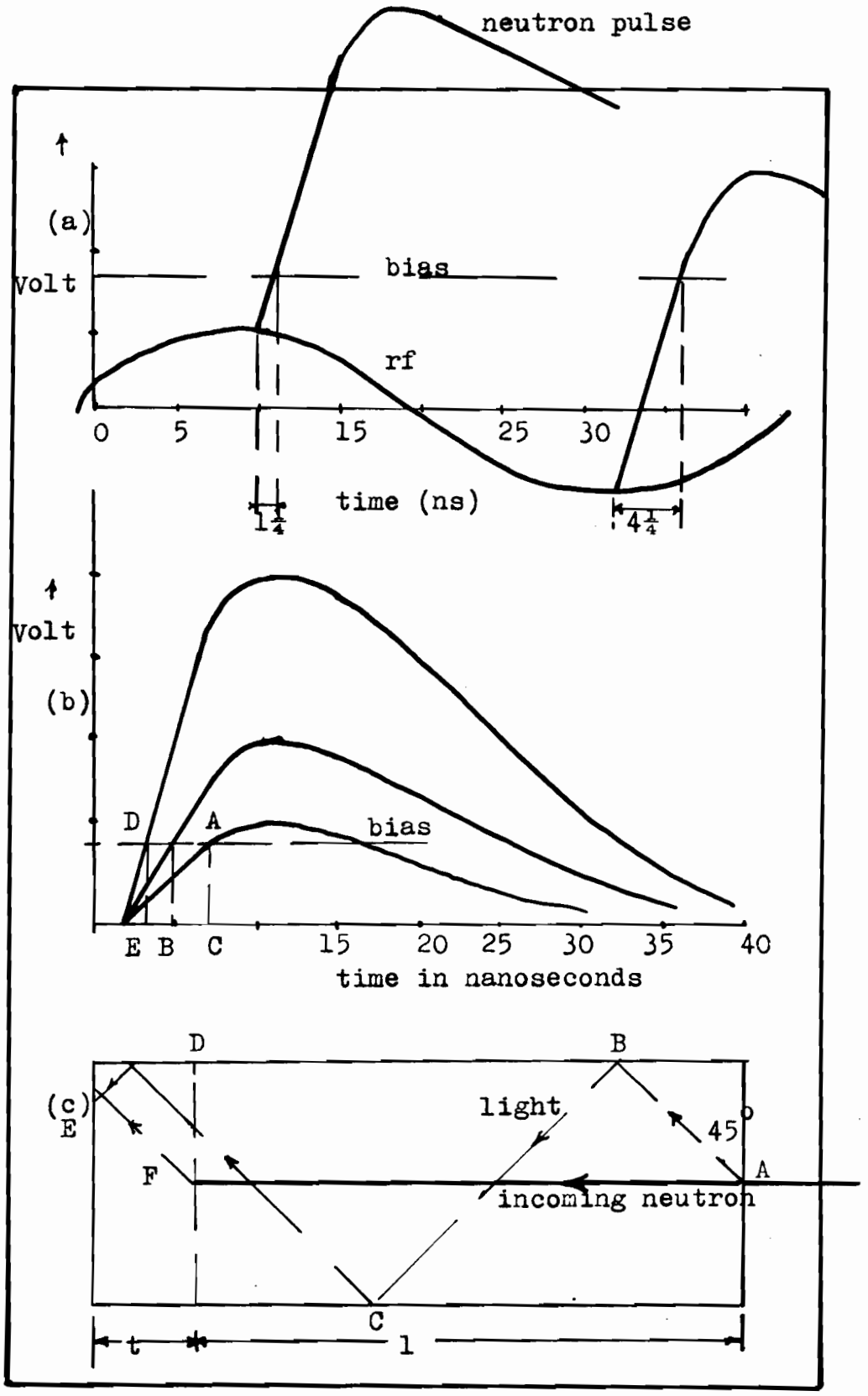
neutron pulse
(a)
volt
bias
rf
0
5
15
25
30
time (ns)
1¼
4¼
volt
(b)
D
A
bias
E B C
15
20
25
30
35
40
time in nanoseconds
D
B
(c)
E
light
45°
F
A
incoming neutron
C
t
l

FIG 6

10 to 90% of maximum, of 8 nanoseconds, the jitter due to the presence of a half volt of pickup would be 0.8 nanoseconds. In the present case, the pickup was reduced to about a tenth of a volt by the use of a clipping line of the appropriate length at the output of the detector emitter-follower.

2.7.3 Time Spread Due to Varying Height of Neutron Detection Pulses

As pointed out in para. 2.6, the height of a pulse in the plastic scintillator which is directly proportional to the energy of the recoil proton, may take on any value between zero and that equivalent to the full energy of the incident proton. Hence if we reject signals for which DA in Fig. 6b is greater than 90% of the maximum voltage, the spread between the time at which the signal from an 80 MeV proton passes the threshold bias B, and that for a 30 MeV proton, will be 5 nanoseconds in the case of the present scintillator. When a 10 MeV window is set at 30 MeV, this variation would be 2 nanoseconds. This figure is reduced to 1.6 by setting the preliminary avalanche discriminator to trigger at 25 MeV.

As mentioned earlier this gives rise to a much lower efficiency for counting neutrons of higher energy than 40 MeV. As the spectrum is richer in high energy neutrons, this constituted no disadvantage in the present case. An alternative method of detection giving pulses of constant slope from the photomultiplier would eliminate this time spread. However the pulses so obtained are small and narrow, thus giving rise to additional forms of jitter later in the circuit.

2.7.4 Electronic Resolution and Miscellaneous Pickup

When two pulses of constant shape and height were fed from a pulser, and separated by a suitable interval, the resolution was found to be about 50 picosecond, and thus negligible. Drifting was also negligible over long periods. ASZ23 transistors operated in the avalanche mode have a constant propagation delay of about 2 nanoseconds as long as the driving pulse is broader than this value at the trigger voltage. It is not desirable to use extremely narrow pulses, nor pulses whose amplitude is barely above the triggering value. Under such marginal conditions (e.g., biassed within 1 mV of the peak of a signal of 5 nanosecond half-width) propagation delays of up to 20 nanosecond may

occur. Biassing the discriminator to trigger on 25 MeV pulses ensured that conditions would not be marginal at 30 MeV, the bottom of the range used. Pickup in any part of the circuit tends to broaden the time spread. Calibration with 100 MeV protons gives the overall resolution including all effects except those discussed in paras 2.7.2 and 2.7.3. In this case there is little variation in the height of the scintillator pulse, and the radio frequency is so phased with respect to the proton as to cause a slight asymmetry in the time structure of the peak. However the beam is not truly monoenergetic, the half-width of the energy peak being about 1 MeV, thus contributing .35 nanosecond to the apparent time resolution.

2.7.5 Effect of Scintillator Length

In Fig. 6c, a crystal of length 'L' is considered, where 't' is the thickness necessary to stop a 30 MeV proton (these are the slowest protons accepted). We shall consider the time taken for light generated by a recoil proton produced at A to reach the photomultiplier tube, as compared with the time required for a neutron of 30 MeV to travel to point F, plus the time for light to pass from F to the tube. Since the photocathode has a detection

efficiency of about 10%, the photon coming by the most direct path will not necessary be the first one detected. Taking the average path as ABCDE, the difference between the two times is:

$$-\frac{1.414\ L}{c/n} + \frac{L}{\beta} + \frac{1.414\ t}{c/n}$$

where β is the ratio of the proton velocity of light in free space, c, and 'n' is the refractive index of the plastic. For a scintillator four inche long and having a refractive index about 1.5, this time difference will be about 0.4 nanosecond.

If each of these contributions is assumed to have a Gaussian distribution, and hence to compound as the sum of the squares, the contribution due to the time structure of the proton burst is dominant, the overall resolution being a little larger than this.

2.8 Inscatter Correction

The neutron detector sees those neutrons which have passed through the absorber unscattered, plus neutrons singly scattered into the 0^{o}-direction, plus a negligible number of neutrons which have undergone multiple scattering.

The absence of a hardening effect can be checked by using different lengths of absorber to demonstrate that the absorption obtained is an exponential function of length.

The optimum location of the absorber is half-way between neutron generator and detector. This location was not available in the present case and the choice remaining lay between having the absorber 8 feet or 3 feet from the detector. In the latter case the absorber is inserted in the collimator and presents only a small projected area to the regenerative extractor, considered as a strong source of spurious neutrons. For this reason this was the preferred location.

When the absorber is small compared with the lengths to neutron source or detector the apparent relative decrease in the total cross section from its true value $\frac{\Delta\sigma_T}{\sigma_T}$ due to the singly inscattered flux (16) is:

$$\frac{\Delta\sigma_T}{\sigma_T} = \frac{\pi \; DL}{4 \; (L_1 L_2)^2} \frac{\sigma_n(0^\circ)}{\sigma_T}$$

L distance from neutron generator to detector

L_1, L_2 distances from absorber to neutron generator and detector, respectively

D	diameter of the collimator
σ_T	total cross section in barns
$\sigma_n(0^\circ)$	cross section for scattering into the 0°-direction in barns/steradian

Since the factor multiplying the ratio of cross sections is less than 10^{-6} the correction is evidently negligible.

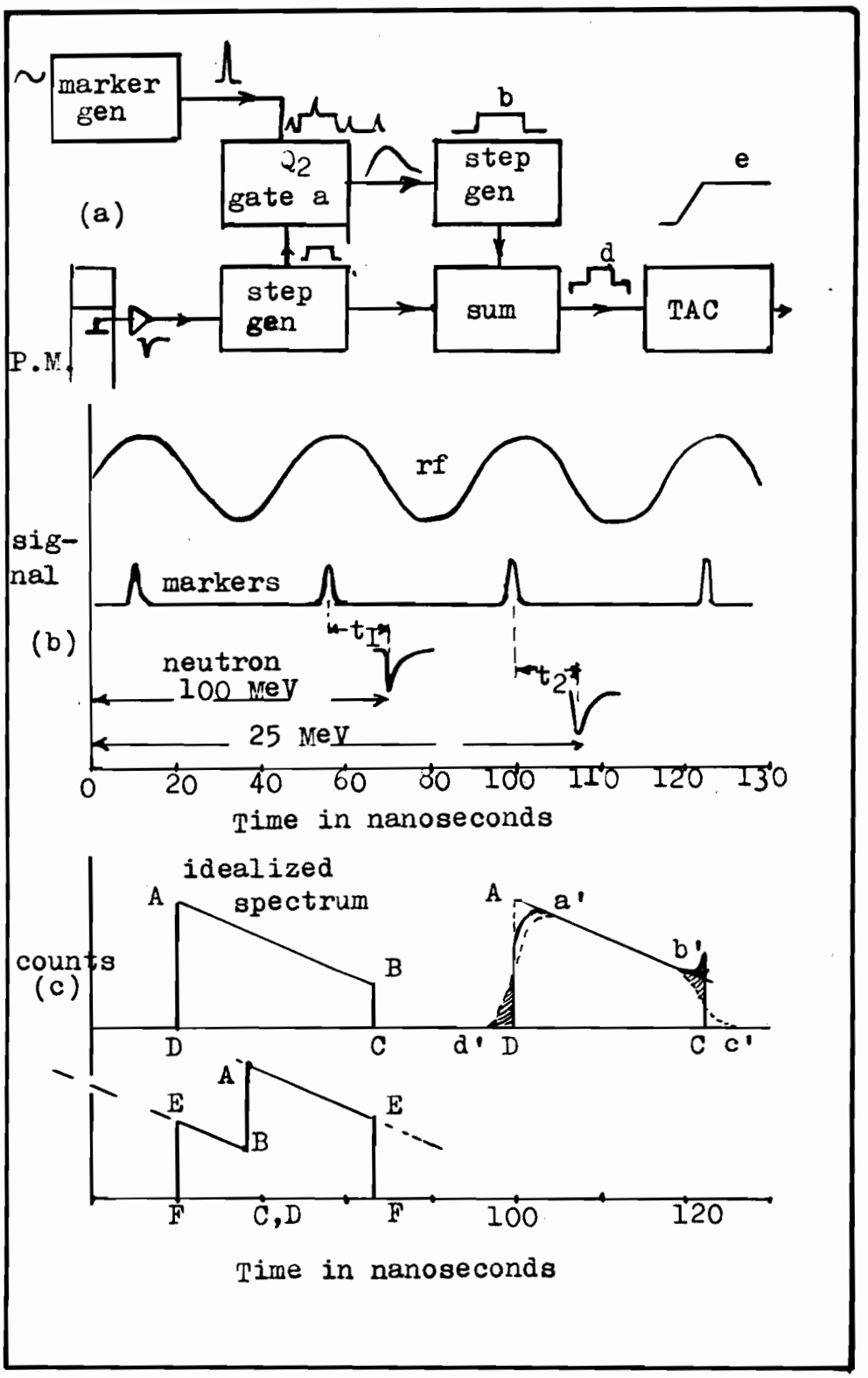
marker gen
b
Q2 gate a
step gen
e
(a)
d
step gen
sum
TAC
P.M.
rf
signal
markers
(b)
neutron 100 MeV
25 MeV
0 20 40 60 80 100 110 120 130
Time in nanoseconds
idealized spectrum
A
B
counts (c)
D
C
d'
a'
b'
c'
E
F
C,D
100
120
Time in nanoseconds

FIG 7

3. ELECTRONIC CIRCUITRY

The overall block diagram was given earlier. Fig. 7 shows schematically the method of time measurement. A 100 MeV neutron associated with the marker B, derived from the radio frequency field of the dee, will evidently arrive at the detector at the same time as a 28 MeV neutron associated with the previous marker. Neutrons of energy greater than 28 MeV can not give rise to such ambiguity, hence an avalanche discriminator and a fast-slow coincidence system are used to eliminate counts due to low energy neutrons. The lengths of the leads connecting the radio frequency pickup and the neutron detector to the time-of-flight apparatus can be adjusted for the most favorable presentation of the spectrum. Fig. 7b shows the cyclic effect associated with changing either lead length. If ABCD is the true shape of the spectrum when the time resolution is zero, the spectrum obtained with non-zero resolution would be a'b'c'd', apart from the cyclic effect of time displacements. The latter results in the spread at the high energy end of the spectrum being added in at the low end of the spectrum, and vice versa. When the true spectrum is peaked at the high energy end as in

our case, this gives rise to a spurious peak at the low energy end of the spectrum. That is, the whole of the 46 nanoseconds between radio frequency bursts is not usable for time-of-flight measurements, but only about 36 nanoseconds when the half-width of the rf structure is 5 nanoseconds. For this reason, an aluminum target was used as the neutron generator since this would not give rise to many neutrons in the energy range 80 to 100 MeV.

As shown in Fig. 7c, the radio frequency marker signal at a is gated by a signal from the main avalanche discriminator Q_1. The output of this gate is fed to a current switch to generate a step-pulse b which is added to the step-pulse from Q_1 as at d. The time-overlap of these pulses is then converted to a voltage in the time-to-amplitude converter as shown at e. After further gating in the slow part of the circuit, using a dynode pulse from the main detector to ensure that only pulses from recoil protons with energy between 30 and 40 MeV can operate the measuring system, the output is analyzed in a kicksorter. The circuitry is conventional apart from the use of avalanche transistors as fast discriminators and as limiters

for generating the step pulses used in the coincidence circuit.

3.1 Avalanche Transistor Discriminators

The relevant properties of the transistor ASZ23 when used as an avalanche discriminator are as follows:

a stable operation as a discriminator for pulses greater than about 0.2V, with the region of jitter of the order of millivolts

b constant propagation time through the transistor, except in the jitter region, of 2 nanoseconds, if the driving pulse is broader than 2 nanoseconds at the trigger point.

c output signal constant at 15 V with 1 nanosecond risetime

d intrinsic dead time about 40 nanoseconds.

All of these properties compare more than favorably with either tube or transistorized Schmitt triggers, while the circuitry is considerably simpler. The transistors in the present equipment operated for eighteen months without signs of deterioration.

3.2 Time Measuring Circuitry

Numerous circuits were evolved and tested during this investigation, however the main experimental difficulties were not electronic, the resolution in particular

being a property of the cyclotron rather than of the electronic circuitry. The circuits described were those finally used for measuring the time structure of the proton bursts, and in obtaining neutron total cross sections.

3.2.1 Radio Frequency Marker Generator

A 30 V peak-to-peak radio frequency signal was capacitatively picked off the cyclotron dee and used to develop a marker signal in phase with the 100 MeV protons. Originally this marker was formed directly at the cyclotron so that no more radio frequency energy than absolutely necessary need be piped into the measuring equipment. However the diodes did not survive long in the intense radiation in the cyclotron vault and the unit had to be moved into the control room.

Fig. 8a shows a circuit used for generating pips one nanosecond wide and 3 volts high, using a Boff diode (13) and a 4 inch clipping line. The signal resulting from the diode only without clipping is shown by ABC. OC is about 4 nanoseconds and the sharp transition CD is less than one nanosecond. The resultant of this waveform and its delayed reflection (shown dotted) when the shorted line is added, is

the narrow positive pulse shown below.

Because of uncertainty in propagation time within an avalanche transistor, when such narrow pulses are used, this circuit was later replaced by that in Fig. 8b. The narrow pulse was originally used because the time structure of the proton burst was not known to be as broad as it was later found to be. The width of this marker gives rise to an uncertainty for times very close to either end of the time spectrum, because of the cyclic character of the latter. However when the time-structure of the proton pulse is broad, this gives rise to the same kind of uncertainty so that the region near either end is unusable in any case. The marker may then be almost as broad as the proton time-structure without worsening the situation. In this circuit (Fig. 8b) the series diode is a Boff (step-recovery) diode and the shunt one is a normal fast diode.

3.2.2 Step Generators and Time-to-Amplitude Converter

Negative signals of maximum amplitude 7 V and risetime 8 nanoseconds, are fed via emitter followers in the photo-multiplier box to the avalanche discriminator Q_1 which is current biassed so that the voltage on the base can be set

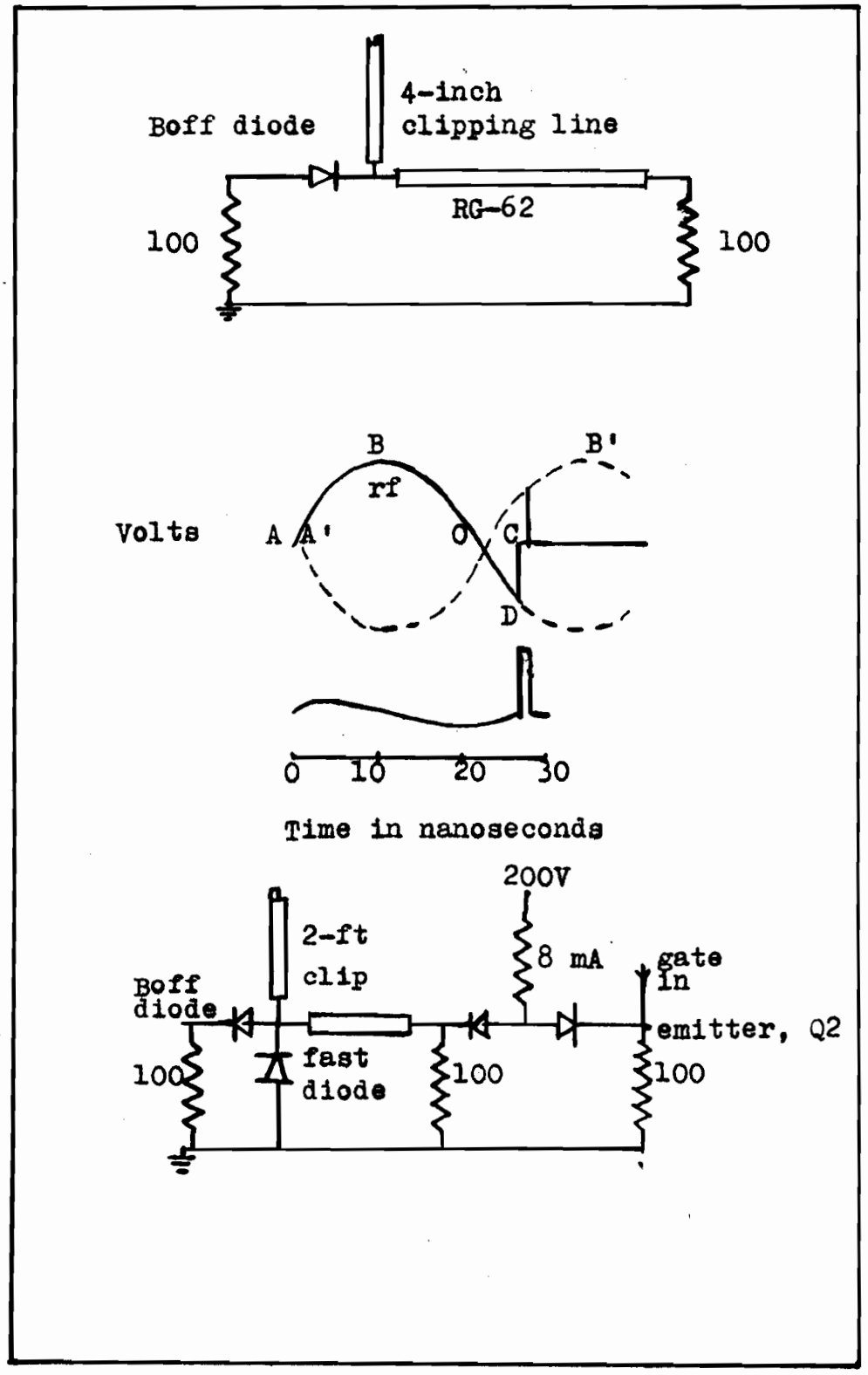
Boff diode
4-inch
clipping line
RG-62
100
100
B
B'
rf
Volts
A
A'
C
D
0
10
20
30
Time in nanoseconds
200V
2-ft
clip
8 mA
gate
in
Boff
diode
emitter, Q2
fast
diode
100
100
100

FIG 8

at any value between 0.2 and 2 volts. An output at B triggers a 15 microsecond univibrator to operate the dead time gate circuit which ensures that the monitor circuit is not counting during the dead time of the timing circuits.

A positive signal from Q_1 goes to a constant current switch based on diodes Y_3 and Y_4. The choke L_1 and the time-to-amplitude converter bias at C, keep the 40 MA current determined by R_1, flowing through Y_3 in the absence of a signal from Q_1. When Q_1 fires, this current is switched through Y_4 into R_2 and the clipping line in parallel with it, thus producing a 2 volt step 60 nanoseconds long.

Another output of Q_1 passes via an emitter follower to a similar current switch based on diodes Y_7 and Y_8 and is added to the rf marker signal which is standardized by the current switch with diodes Y_9 and Y_{10}. The latter is necessary in order to isolate the marker-forming circuit, with its highly non-linear impedance, as a function of time from the rest of the circuitry. The diode consisting of the base and emitter of Q_2 is so biassed as to conduct only when both marker and positive step are present, in which case Q_2 avalanches. The positive signal so obtained is

shaped by current switch Y_{13}, Y_{14} and added on R_2 to the step derived from the neutron pulse. When the sum pulse exceeds a suitable bias it switches the current normally passing via R_4 through R_2 into the condenser to give a signal, the amplitude of which is proportional to the time of overlap. Q_3, Q_4 and Q_5 shape and amplify the signal to make it suitable for operating the kicksorter.

In general, current switches are used both to provide flat-topped pulses of standard amplitude, and to provide isolation between parts of the circuit the interaction of which would be detrimental. In particular, when Q_1 fires, Q_2 would also fire, even before the marker arrived, if it were not for the isolation provided by an emitter follower and a current switch. These devices are intrinsically very fast because ideally, there is no current change when the current is switched from one side to the other side of the circuit. The maximum speed could not be utilized here, as diodes which switch faster than one nanosecond cannot stand off reverse voltages greater than two or three volts. Thus diodes with 2 nanosecond switching time were used as these will not be damaged by the large signal put out by avalanche transistors.

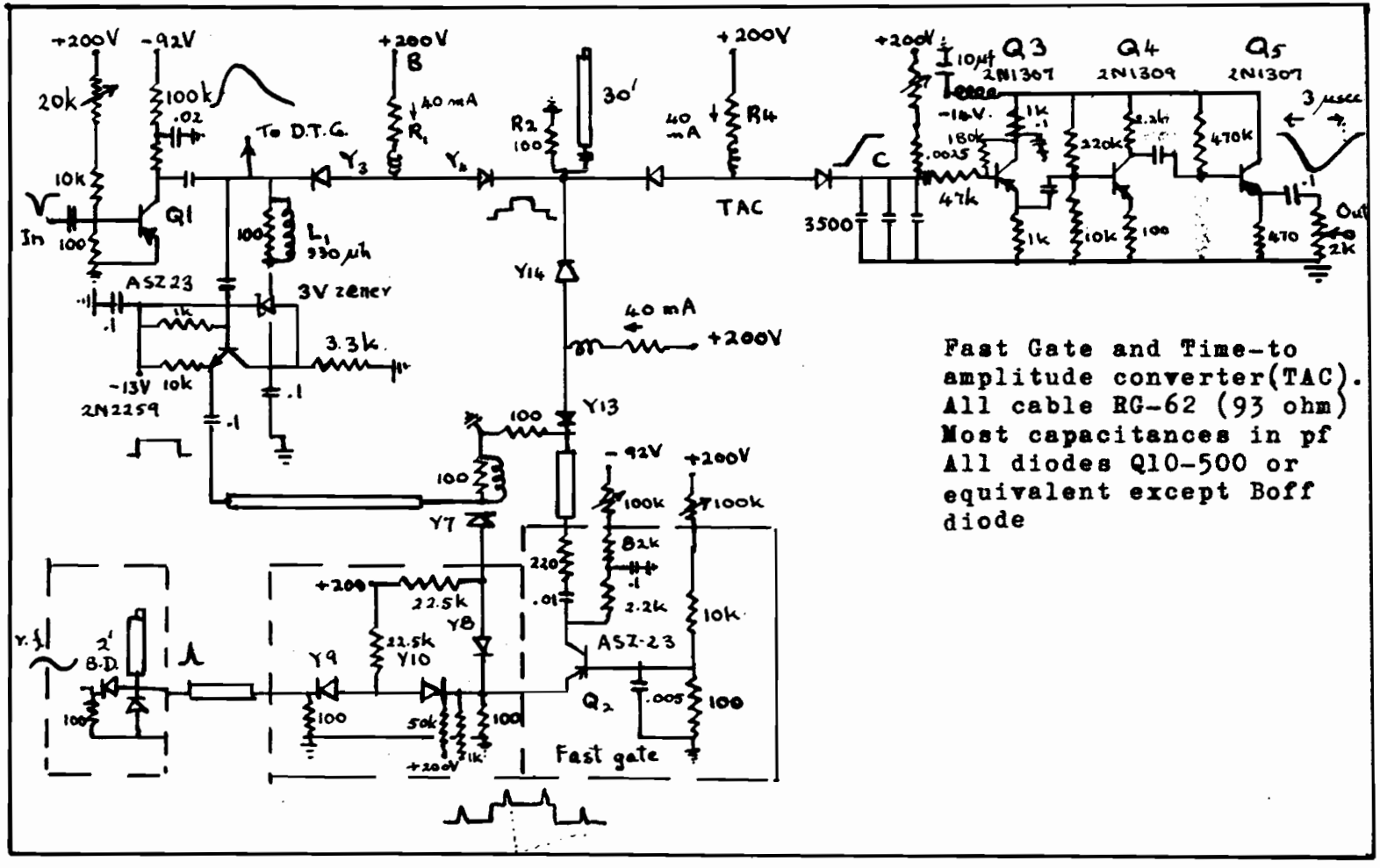

Fast Gate and Time-to amplitude converter(TAC). All cable RG-62 (93 ohm) Most capacitances in pf All diodes Q10-500 or equivalent except Boff diode

FIG 9

3.3 Linearity of the Time Analyzing Circuit

Factors causing departure from linearity in the timing aircuit are in certain cases, such as radio frequency pickup, the same as those already discussed in connection with the question of energy (hence time) resolution. Here we shall discuss three specifically electronic contributions to nonlinearity which are characteristic of the circuit used.

3.3.1 Time-to-Amplitude Converter Circuit Ringing

Fig. 10a shows the TAC condenser being fed by a constant current from R, when the bias exceeds E_A. The diode switching time is 2 nanoseconds, hence for a standing current of 20 mA, the rate of current change is about 10^7 amp/sec. The leads to the condenser act as inductors of a high-Q ringing circuit, which in practice continues to ring for the 50 nanoseconds that the current may flow. The stretched amplitude evidently depends on whether stretching began at a peak or a trough of the sine wave modulating the ramp.

3.3.2 Effect Due to Gate Pulse Shape

Fig. 10b shows in an exaggerated form, the time error introduced if the gating pulse is not perfectly flat. In

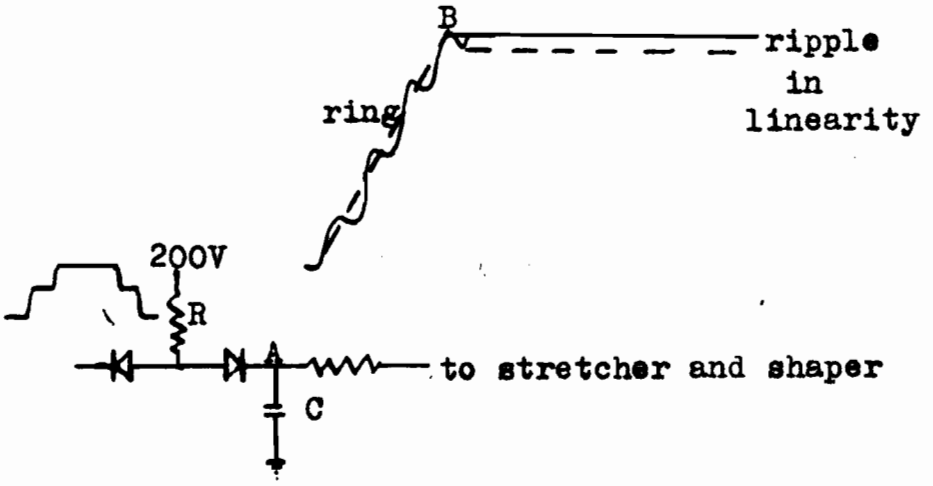

(a) Effect due to ringing of TAC condenser

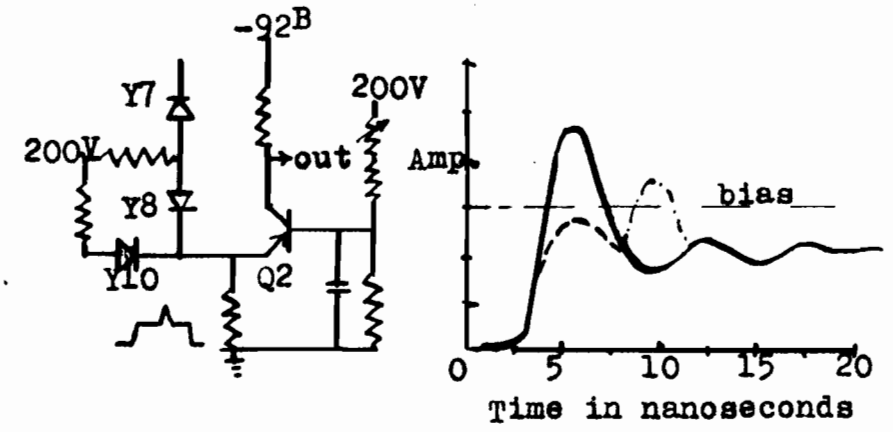

(b) Effect due to shape of gate pulse

FIG 10

fast circuits, the natural resonances of components give rise to small rings whenever the current is changed, hence it is virtually impossible completely to eliminate fine structure from the gating pulse to which the marker is added. As in the case of radiofrequency pickup discussed before, this causes a small variation in the time at which the discriminator is triggered. In addition there is some capacitative feedthrough with diodes Y_7, Y_8m which gives rise to a peak at the front of the step, and which is very noticeable on the differential linearity curve shown in chapter 4, on the right hand side, since this occurs where there is the greatest overlap of the pulses.

3.3.3 Effect Due to the Shape of the Sum Step Pulse

For reasons similar to those already discussed, deviation of the top of the pulse from a flat form causes nonlinearity in timing, since the time taken for the voltage at the end of the step to drop to the bias voltage will vary when there are bumps on top.

All the effects described above can be minimized by using very fast-rising pulses. Because of the inherent speed of the avalanche process and the use of current switches, it was easy to hold the risetimes

to a few nanoseconds, and rings of this nature to about 10% of the pulse amplitudes, so that 0.2 to 0.4 nanosecond fluctuations could be expected. The various effects are of course cumulative, the main contribution arising during gating of the rf marker pulse. Circuitry similar to the present has been used by Hardy (14) with an ultimate resolution of 0.4 nanosecond and excellent integral linearity. However, neither of the timing pulses was gated, nor was there a heavy rf background. Owing to the periodic character of the calibration, the time range can be shifted by putting delays in either the radio frequency signal lead or the neutron lead to move the gross nonlinearity at the right hand side away from an energy range of special interest.

3.4 Dead Time Gate and Counting Circuits

To eliminate computed corrections, a dead time gate was employed to ensure that the monitor scaler counted only when the time-of-flight equipment was live. Because of the long dead time of the kicksorter, tens to hundreds of microseconds, not more than one neutron could be timed during any 10 microsecond burst. The circuitry was thus adjusted to have a fixed dead time of 15 microsecond, and a gate of this

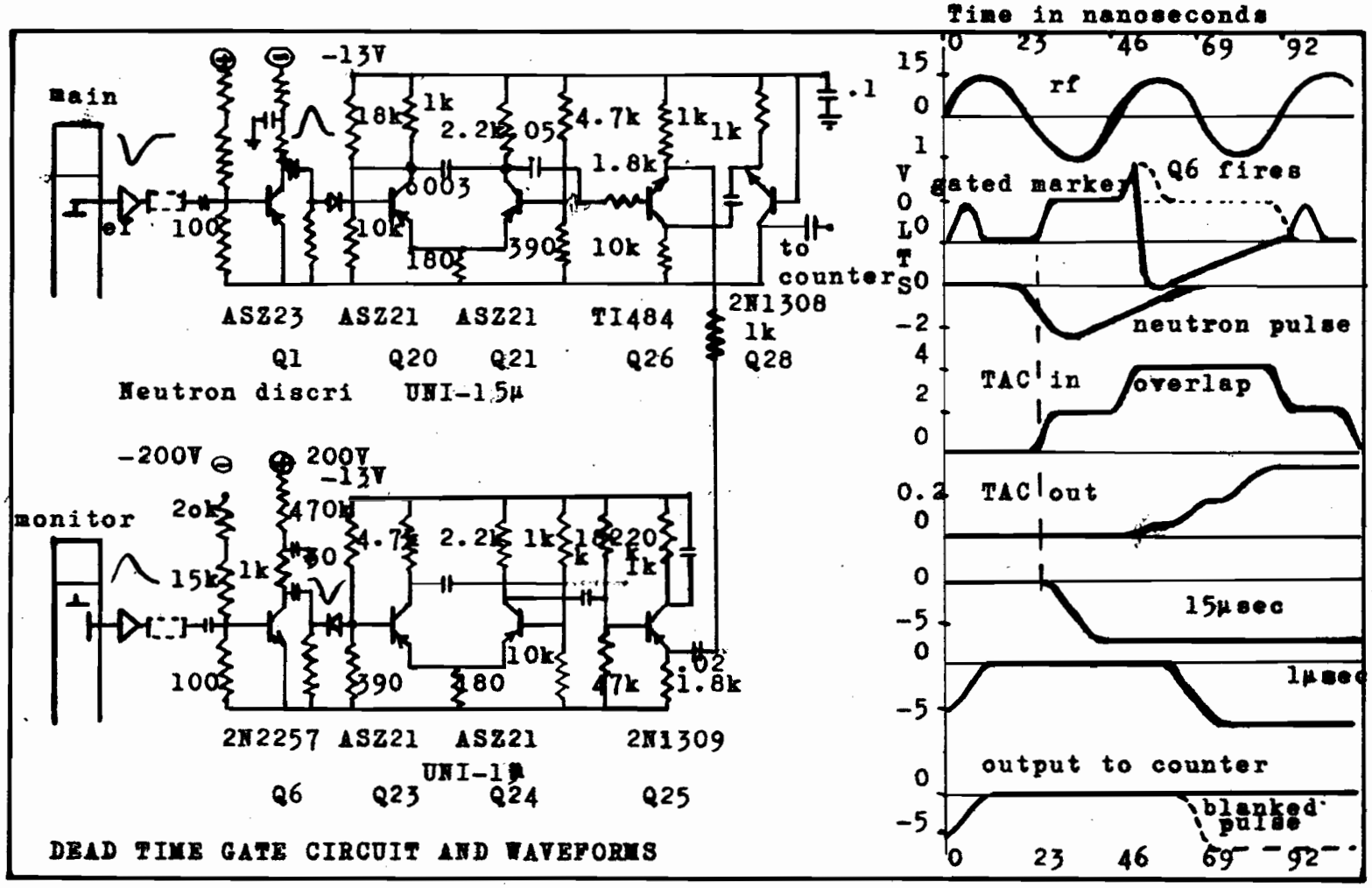
Time in nanoseconds
0
23
46
69
92
main
-13V
1k
18k
2.2k
.05
4.7k
1k
1k
.1
1.8k
.003
100
10k
180
390
10k
to counter
2N1308
1k
Q28
ASZ23
ASZ21
ASZ21
TI484
Q1
Q20
Q21
Q26
Neutron discri
UNI-1.5μ
-200V
200V
-13V
monitor
20k
470k
15k
1k
4.7k
2.2k
1k
220
1k
.02
10k
100
390
180
47k
1.8k
2N2257
ASZ21
ASZ21
2N1309
UNI-1μ
Q6
Q23
Q24
Q25
DEAD TIME GATE CIRCUIT AND WAVEFORMS
15
0
1
V
0
L
0
T
S
0
-2
4
2
0
0.2
0
0
-5
0
-5
0
-5
rf
gated marker
Q6 fires
neutron pulse
TAC in
overlap
TAC out
15μsec
1μsec
output to counter
blanked pulse

FIG 11

length was generated by the univibrator using Q_{20},Q_{21}, triggered by one of the pulses from the neutron discriminator Q_1.

A positive pulse from the monitor scintillator was fed to an NPN avalanche discriminator Q_6 (dead time 40 nanoseconds) which triggered a univibrator using Q_{23},Q_{24} to produce a one microsecond pulse, which was then fed to the base of gating transistor Q_{26}. Whenever the dead time gate pulse was present on the emitter of Q_{26}, the transistor was sufficiently cut off, that the pulse from the emitter follower Q_{25} was not able to switch it on again. When the dead time gate was absent, 7V pulses were fed via Q_{28} to a counter of intrinsic resolution one microsecond. Q_6 was biassed so as to count only high energy neutrons, thus keeping the count rate so low that counting losses were negligible. Initially a circuit was built for switching off the kicksorter when the required count was reached, but when the kicksorter was replaced by one of different manufacture, a replacement circuit was not built, since the error involved in manual switching is negligible.

4. EXPERIMENTAL RESULTS

4.1 Time Structure of the Proton Bursts

Approximately 400 times a second, a radio frequency field is applied for 2500 microseconds to the cyclotron dee, protons being emitted for 10 microseconds of this time, in discrete bursts spaced 46 nanoseconds apart. In synchrocyclotrons such as that at McGill, because of the phase stability characteristic, protons can be accelerated over about 120° of an rf cycle, that is they may be emitted for about 15 nanoseconds in each burst. The width of this time structure has been cited as 7, 9, and 11 nanoseconds at half the maximum amplitude, in the case of the Harwell time-of-flight facility. A similar variability has been found in measurements with the McGill cyclotron, depending on the stability of its operation and the length of run. On occasions the half-width remained at 4 nanoseconds for several hours despite variation of cyclotron settings. However, since the type of synchrodetector was changed this year, the best figure was 5 and the mean about 7 nanoseconds. It was found that the structure may be narrow --about 3 nanoseconds with 7 kV accelerating voltage --for short periods of the order of seconds, but the phase of the proton with respect to the radio frequency field sometimes shifts erratically

so that when a peak is accumulated over a rather longer period of time, the overall width at half-height is usually about 7 nanoseconds. For this reason there is not much point in showing a 'typical' peak.

In view of the fact that the width of the peak appears to be narrow considered on a short term basis, it might be feasible to measure this quantity continuously between neutron flight time readings, and use the output signal in a negative feedback system to correct for fluctuations in the relative phase of the proton with respect to the radio frequency field. This assumes that they are due to relatively slowly changing effects such as that due to variation in the rate of rotation of the condenser which controls frequency modulation.

The present system in which the maximum timing cycle is only 46 nanoseconds, suffers from the disadvantage that the resolution is not automatically monitored by gamma bursts from the neutron generator, as was the case in the Harwell system. Such signals, in our case, are below the threshold for detection, as the flight time of a gamma ray would be 45 nanoseconds, and would thus appear near the location of

100 MeV neutrons, which require 70 nanoseconds to cover a distance of 25 feet.

Fig. 12 shows results obtained before the synchrodetector was replaced by an optical synchronizing system. In Fig. 12a the proton pulse is shown with 10 nanoseconds delays inserted in the neutron lead. When the cyclotron is stable, the curve is close to a gaussian shape. In obtaining this curve, the cyclotron was run with 7 kV accelerating voltage and the magnetic field was adjusted so as to reduce the external beam current below 1 picoamp. The current was further attenuated by means of a brass block $\frac{3}{4}$-inch thick, with a No. 50 hole drilled through it. These conditions are rather different from those applicable when neutrons are being generated, principally in that the magnetic field is then optimized for maximum proton output (about 5 nanoamps in recent months, at 7 kV). The time structure under these two conditions should be the same, other things being equal.

Two methods were used for calibration:

a) A delay line, the length of which could be varied in nanosecond increments, was inserted in the radio frequency pickup lead, and the time between rf markers and the signal generated by a 100 MeV proton, was measured.

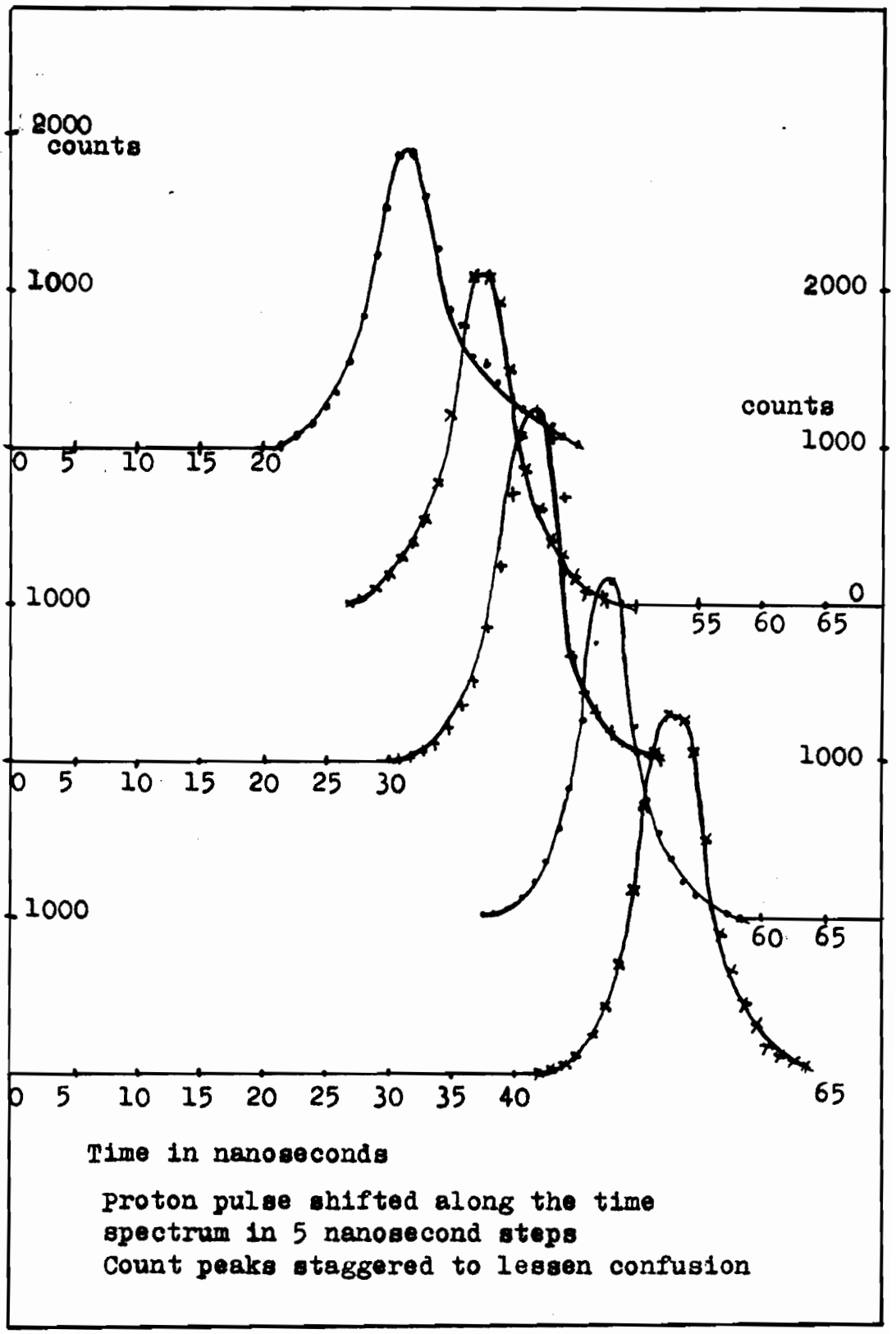
2000
counts
1000
0 5 10 15 20
1000
0 5 10 15 20 25 30
1000
0 5 10 15 20 25 30 35 40
2000
counts
1000
0
55 60 65
1000
60 65
65
Time in nanoseconds
Proton pulse shifted along the time
spectrum in 5 nanosecond steps
Count peaks staggered to lessen confusion

FIG 12

This method is time-consuming and tedious, but has the advantage that the calibration is carried out under conditions substantially the same as those in measuring neutron flight times.

b) The time of arrival of a 100 MeV proton pulse with respect to a 22 Mc signal from a signal generator, not synchronized with the proton, was used to generate a spectrum which should be rectangular if the equipment is linear. This will be discussed later.

In the first method, in addition to obtaining a time calibration, the time structure (and hence the time resolution of the system) is automatically provided as a function of the delay inserted into the lead. Fig. 12 shows such a spectrum, with the proton peak being shifted in four steps, each 5 nanoseconds long. The resolution here varies between 5 and 7 nanoseconds, and in assessing neutron spectra later obtained, the resolution was taken to be fixed at 7 nanoseconds. As explained earlier, the resolution of the present system is in effect equal to the width at half height of this 100 MeV proton peak, since other contributions to the resolution are much smaller.

Linearity was initially measured by introducing a standard pulse from a mercury pulser to one input, and the same pulse, but delayed suitably, to the other input, and measuring the time between the two pulses. This how- does not test the equipment under actual operating conditions and so the two methods mentioned in the last paragraph were also used, a linearity curve thus obtained being shown in Fig. 13. For convenience, the output signal to the kicksorter, was adjusted so that one channel equals one nanosecond.

The other method which takes less time and is thus more suitable for a quick check before carrying out a cross section measurement, involves measuring the time between arrival of a signal of a suitable shape (either from the 100 MeV proton, or from a pulser) and marker pulses from a signal generator which is not synchronized with the other signal. In this case, if for instance, the frequency of the signal generator is 20 Mc, then the maximum time between the apparance of a signal and the arrival of the next marker will be 50 nanoseconds, and since the two sources are statitistically independent, there is equal probability for

the occurrence of all intervals between 0 and 50 nanoseconds, so that a rectangular spectrum as shown in Fig. 13, is obtained. The deviations from a flat curve indicate departures from linearity in the circuit. The ripple on top of the curve is due to ringing of the condenser in the time-to-amplitude converter, as explained in 3.3.1, and the peak at the right side is a gating effect, explained in 3.3.2. Although the circuit was modified on numerous occasions during development, the differential linearity curve was always similar to this one, indicating linearity for all except the last few channels at the right, as within 5% (for one nanosecond increments) in agreement with the direct method of measuring linearity by varying the delay between the cyclotron rf marker and the 100 MeV proton.

The stability of the overall system, including the cyclotron, was such that there was never more than one nanosecond drift in the total range, and as this effect is immediately obvious as a translation by one channel of the kicksorted spectrum, or by a compression or expansion of the same, it could easily be allowed for. The effect of the time structure of the proton burst does not show in this

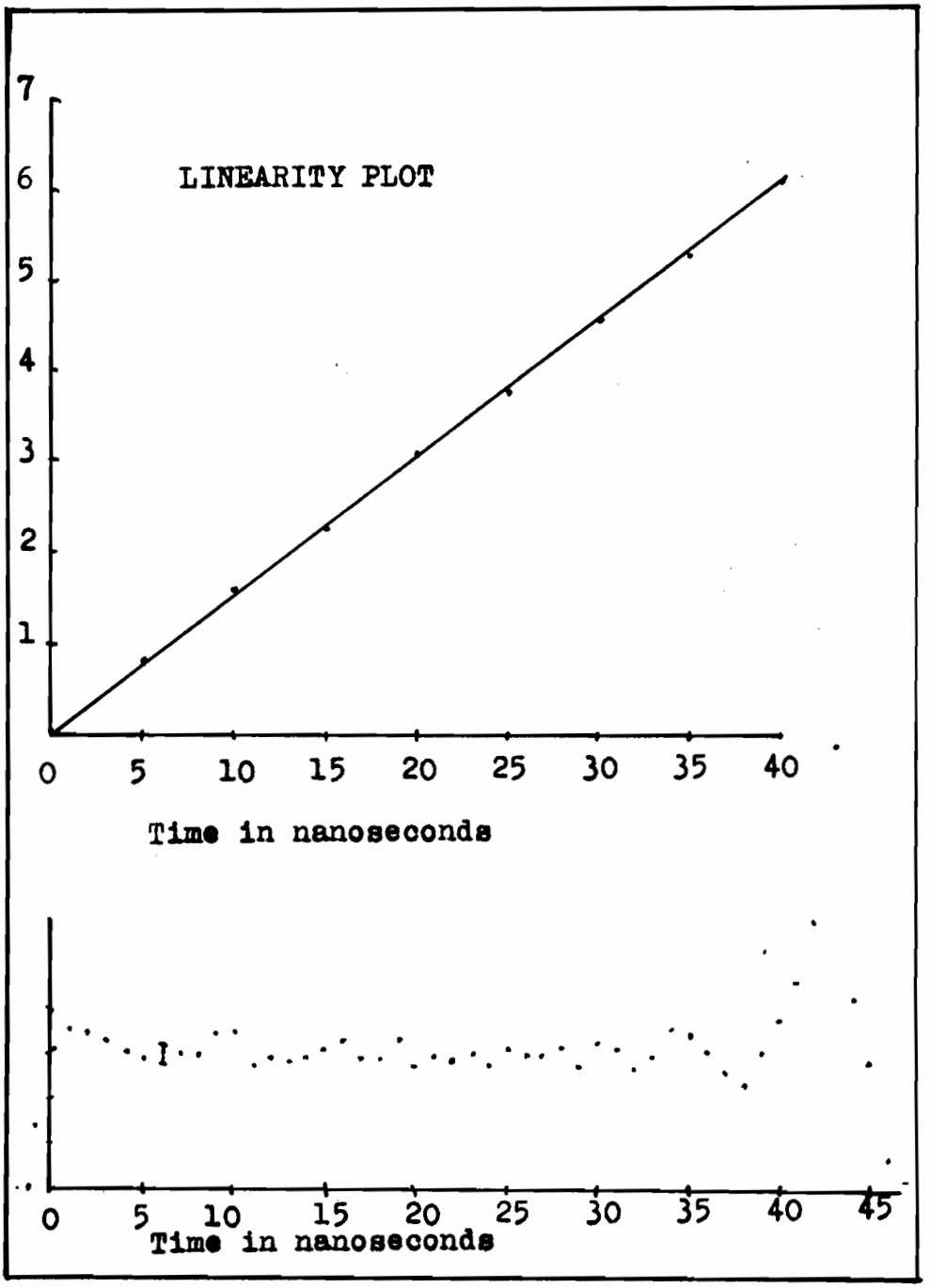
LINEARITY PLOT
7
6
5
4
3
2
1
0
5
10
15
20
25
30
35
40
Time in nanoseconds
0
5
10
15
20
25
30
35
40
45
Time in nanoseconds

FIG 13

spectrum because of its cyclic nature. That is, the spectrum cuts off sharply at each end, the shape being the same as if the system resolution were zero. When the spectrum is not 'white', that is, flat-topped, its shape is distorted as mentioned before, counts due to 30 MeV protons, delayed with respect to the rf marker being transferred to the 100 MeV end, and vice versa for early 100 MeV protons.

The sharp cutoff at both ends of the spectrum obviously indicates that: 1)electronic resolution is much better than one nanosecond; 2) the gating avalanche, Q_2 always fires when the first gated marker pulse appears at its emitter. If there were variation in the propagation time of Q_2, the ends of the spectrum would be diffuse, and if Q_2 did not fire on the first gated marker, the spectrum would extend the full length of the gate pulse, (about 100 nanoseconds).

4.3 Neutron Total Cross Section Measurements

As discussed previously, neutron total cross sections are obtained by measuring neutron flux as a function of energy with an absorber obstructing the beam, and when it is removed. In order that the results be meaningful, the neutron spectrum incident on the detector should be the same in both cases. In practice, great difficulty was

encountered in ensuring that this was the case.

It was originally intended to monitor the total integrated flux by counting neutrons incident on a plastic scintillator detector, situated 5^{o} away from the direction of the main detector. To ensure that the presence or absence of an absorber would have no effect on the monitor count-rate, the absorber was inserted entirely within the end of the iron collimator. The signals from this monitor were gated by means of a dead time gate derived from signals produced by the main detector, so that the monitor counted only when this circuit was live. The counting rate was sufficiently low that counting losses could be neglected. When a subsidiary monitor was used, it was found that this scintillator monitor was not satisfactory as:

a) the number of counts registered for a given total flux of neutrons, drifted slowly in the course of a run;

b) random, short term fluctuations occurred. These effects are believed due to:

a) shifting of the apparent detector threshold with time due to a changing pile-up effect as the concrete block in which the detector was situated, became radioactive;

b) due to inadequate collimation of the beam entering

the monitor which could 'see' neutrons having a spectrum which fluctuated more than those entering the main detector.

For the above reasons, monitoring the neutron flux was later carried out by integrating the current of protons having their energy degraded to less than 30 MeV on passing through the neutron generator, by means of a Faraday cup (designed and built by Per Portner) placed about 10 feet from the neutron generator. Because of angular spread in the degrading process, only about 2/3% of the initial flux at the neutron generator, was collected here, and since neutrons generated by 30 MeV protons would be below the threshold of the time-analyzing equipment, they introduce no direct error. The proton current received here was integrated and a run would continue for the time necessary to collect from 2.5 to 50 nanocoulomb. Leakage of the integrating circuit was negligible during a run, however another effect was sometimes found to be embarrassing. Fig. 14 shows schematically the location of the cup with respect to the neutron generator and detector. There are collimating slits located directly ahead of the cup, and it was impossible to use the latter as a monitor after a run in

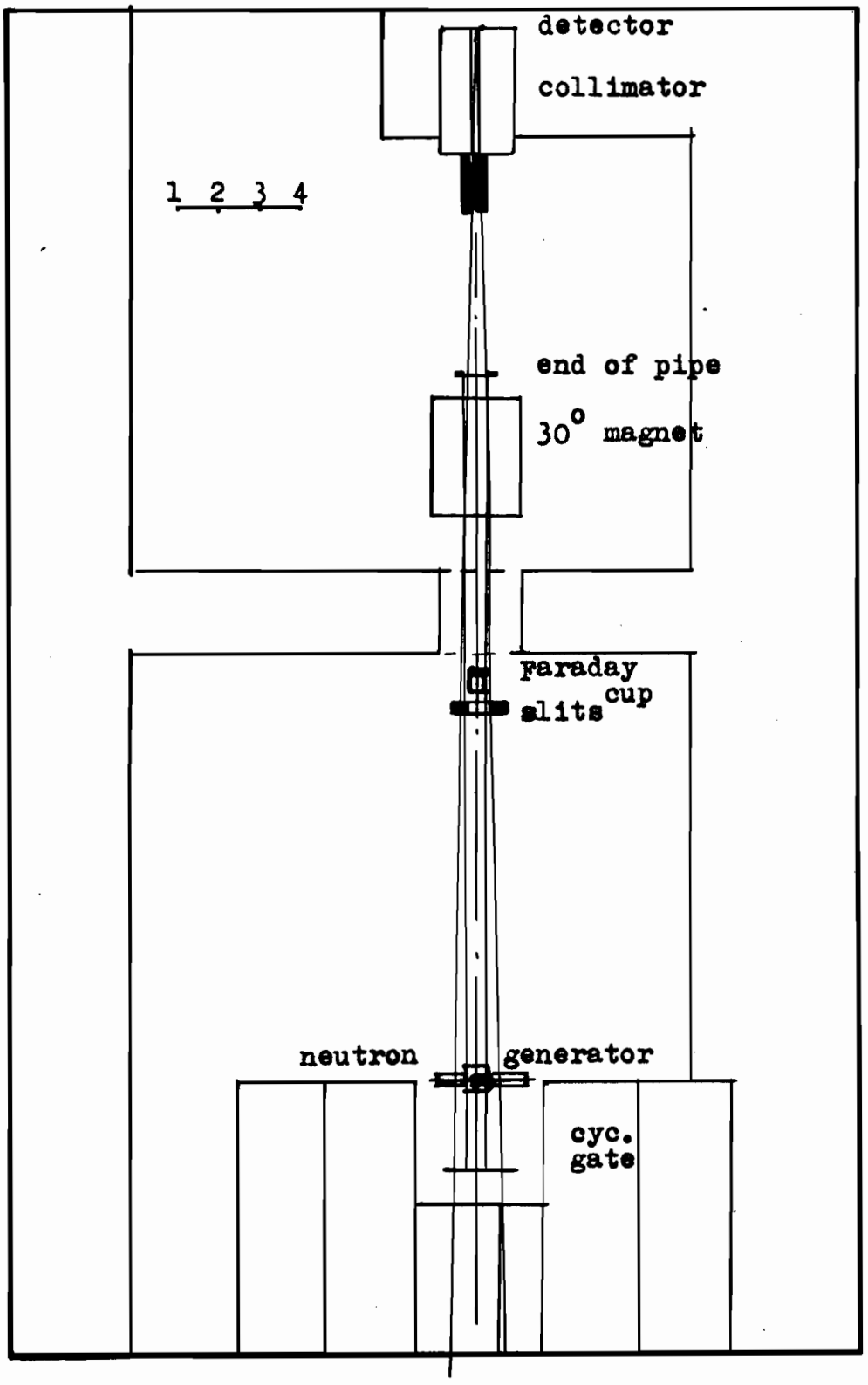
detector
collimator
1 2 3 4
end of pipe
30° magnet
Faraday cup
slits
neutron generator
cyc. gate

FIG 14

which the slits had been subjected to heavy bombardment for a long time. Slot positron activity (the jaws are made of brass)was such that the charge collected was as high as 3.6 picocoulomb per second after a four hour run with an external beam current of one nanoampere. The mean life of the activity was about 30 minutes.

The other problem mentioned above --that of ensuring that the same energy spectrum is being measured throughout a run gave considerable difficulty because of the geometry of the layout shown in Fig. 14. By opting to carry out this experiment in the cyclotron vault in the vain hope of completing it before the beam hall was completed, freedom to select an unobstructed flight path was lost as there was only one practical location for the neutron generator and flight path. The former was located just beyond the cyclotron gate to the external beam and in an evacuated four-inch diameter pipe through which protons normally travel to the steering magnets. As it was believed that the external beam would not be more than about one inch in diameter, the neutron generators were made 1⅛ inch square (and 70 MeV thick) so as to be retractable into

two-inch diameter side arms. In fact although most of the beam is within this area there are many protons off the central axis the flux of which is not as stable as that of the central protons. Such protons which are not intercepted by the neutron generator, but by obstructions considerably closer to the monitor (and thus making a larger solid angle with respect to the latter) give rise to a distortion of the time-of-flight spectrum which is also liable to fluctuate. This arises because the neutron beam cannot be collimated to a smaller diameter than the four-inch pipe in which it is travelling, until it emerges from this pipe fifteen feet away from the neutron generator.

The main collimator and shielding for the detector consisted, as described in para 2.5, of a pile of iron, three feet deep in the direction of the beam and pierced by a hole of one inch diameter. The area in the plane of the neutron generator thus seen by the main detector is equivalent to a circle eight inch in diameter. At the Faraday cup and slits, the circle seen is five inch in diameter, thus allowing much scope for the production of neutrons there.

It is not considered that neutrons generated in the cyclotron, where 99% of the internal beam protons are lost at the regenerator, would be likely to contribute greatly to this spectral distortion because of the geometry and the fact that neutrons having energy less than 30 MeV are not accepted by the time analyzing equipment. An additional collimator was placed ahead of the main one so as to reduce the area seen at the neutron generator to that of a circle less than two inch in diameter, whereupon there is no obstruction between this point and the detector when the slits are wide open. The collimator was an eighteen inch iron cylinder pierced by a hole of 23/64" diameter.

4.4 Experimental Procedure

By means of aluminum degraders, the main and monitor photomultiplier detectors were calibrated with protons at a suitable voltage, finally fixed at 1375 V. The avalanche discriminators were biassed to trigger on 25 MeV protons. The time-of-flight pulses were then, after time-to-amplitude conversion and shaping, gated by pulses derived from a dynode of the main detector so as to accept only those associated with recoil protons having greater energy than 30 MeV. The spectrum in Fig. 15 shows the

characteristic shape, peaked at the high energy end (conventionally at the left in time-of-flight spectra). The peak at the right hand side is an electronic effect due to gating. The same spectrum after a 10 MeV window is applied, is shown in the lower part of the figure. The high energy peak is almost eliminated. Note how sharply the spectrum terminates on both sides, thus indicating that purely electronic resolution is small.

In commencing a run, the differential linearity was checked by timing the cyclotron protons with respect to a nonsynchronized signal from a signal generator. The location of the 100 MeV proton on the spectrum was checked, and if it were not at the left hand side, a length of cable was added to move the peak to this point. A neutron time of flight spectrum was then recorded to check that the 100 MeV point was indeed at the origin. Then the neutron generator was inserted in the beam path and counts were taken with and without the presence of an absorber, for a time determined by the integrated charge collected on a Faraday cup intercepting the neutron path. Only 2/3% of the original proton flux reached the cup due to spreading of the proton beam during the degrading process.

This verifies that most of the beam was indeed intercepted by the neutron generator. The number of counts received by the monitor was recorded, and the time taken to accumulate the fixed charge was noted, as a check against stability of cyclotron operation.

The ungated count rate was 10 per second hence counting losses were negligible. As the solid angle subtended at the detector was less than 10^{-6} steradians and the distance between absorber and detector 51 inch, no inscatter correction was necessary. Fig. 16 shows spectra for a 1½ inch and a 3 inch absorber, the attenuation scale for the 1½ inch length being the square root of the scale for the 3 inch piece. This demonstrates that there is no spectral hardening during tansmission.

The background was measured by means of an infinite absorber (a four foot iron rod plugging the main collimator) and found to be ¼% of the count rate when the hole was clear. Consequently the cross section could be obtained by direct application of the formula. The runs, alternating absorber in and out, were ten to thirty minutes long, the copper spectrum shown in Fig. 17 requiring six hours in all, in-

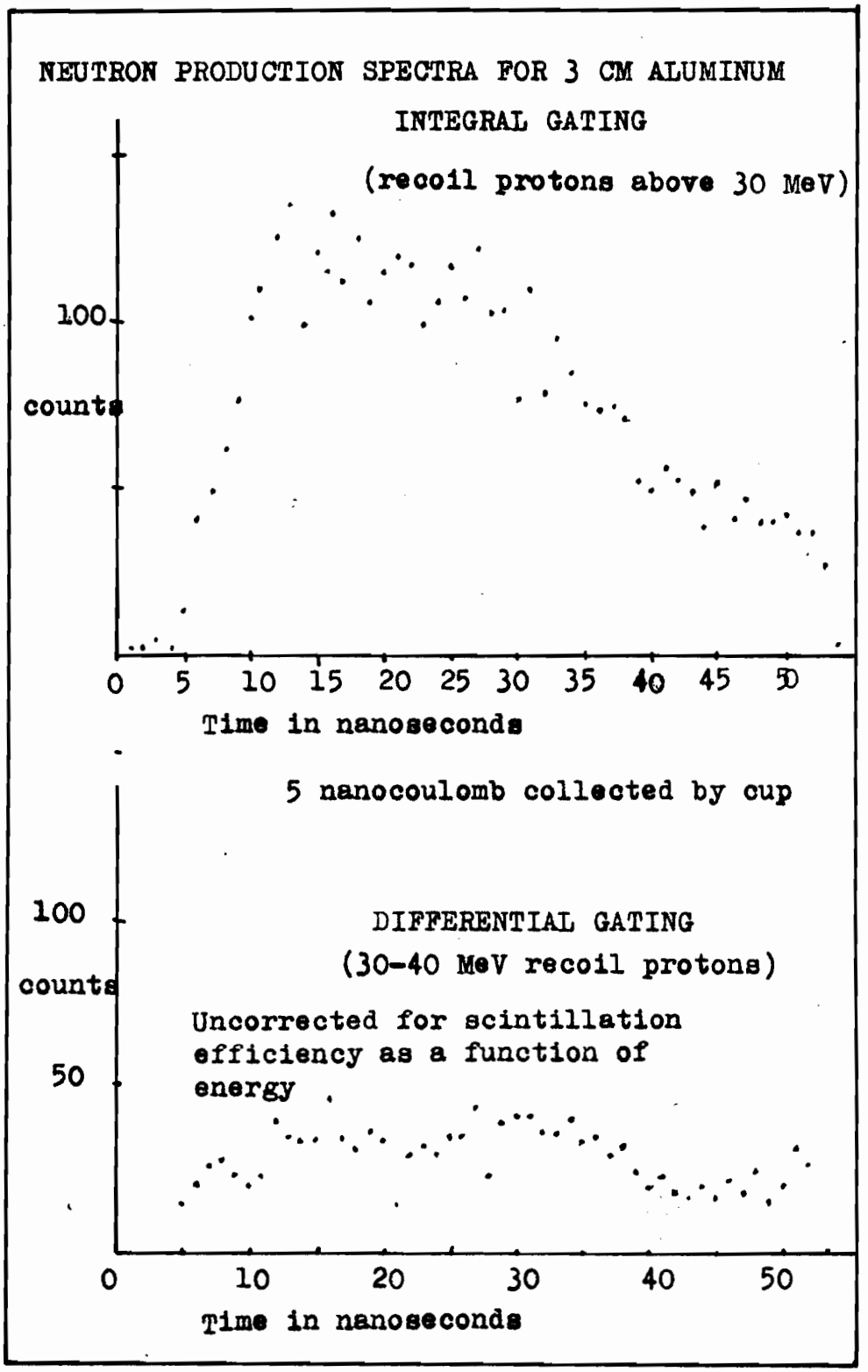
NEUTRON PRODUCTION SPECTRA FOR 3 CM ALUMINUM
INTEGRAL GATING
(recoil protons above 30 MeV)
100
counts
0 5 10 15 20 25 30 35 40 45 50
Time in nanoseconds
5 nanocoulomb collected by cup
DIFFERENTIAL GATING
(30-40 MeV recoil protons)
Uncorrected for scintillation efficiency as a function of energy
100
counts
50
0 10 20 30 40 50
Time in nanoseconds

FIG 15

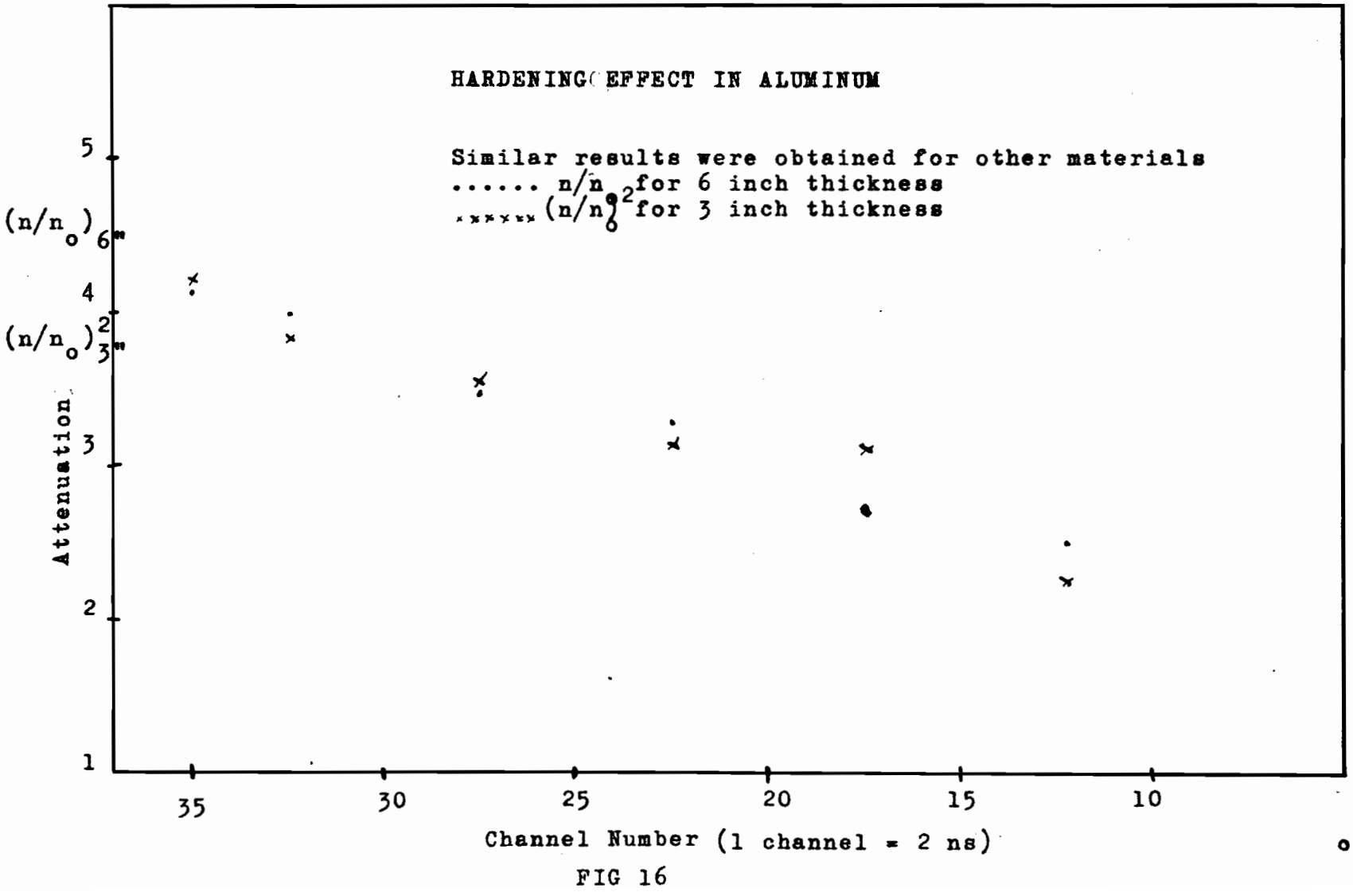
HARDENING EFFECT IN ALUMINUM
Similar results were obtained for other materials
..... n/n_o for 6 inch thickness
xxxxxx (n/n_o)^2 for 3 inch thickness
(n/n_o)
(n/n_o)^2/3
Attenuation
5
4
3
2
1
35
30
25
20
15
10
Channel Number (1 channel = 2 ns)

FIG 16

cluding checking of time scales, etc. The statistical error is about 4% on each point and no corrections have been applied.

4.5 Experimental Results

The channels of the kicksorter were set to be equivalent to one nanosecond each, but in calculating results, the counts were integrated over 7 nanosecond intervals in view of the width of the rf structure of the incident protons.

The absorbers were in all cases cylinders of one inch diameter. No coating was applied to the calcium to protect against oxidation. Instead it was kept immersed in kerosene between runs so that the amount of oxidation that occurred was unimportant. The potassium was packed into a one-inch diameter brass cylinder and kept between runs either in kerosene, or, with the ends coated with paraffin wax, in a desiccator. It was found necessary to cut off the ends freshly before each run, and reweigh it.

To compare the performance of the equipment with that of other workers, the cross section for copper was also measured, excellent agreement being obtained

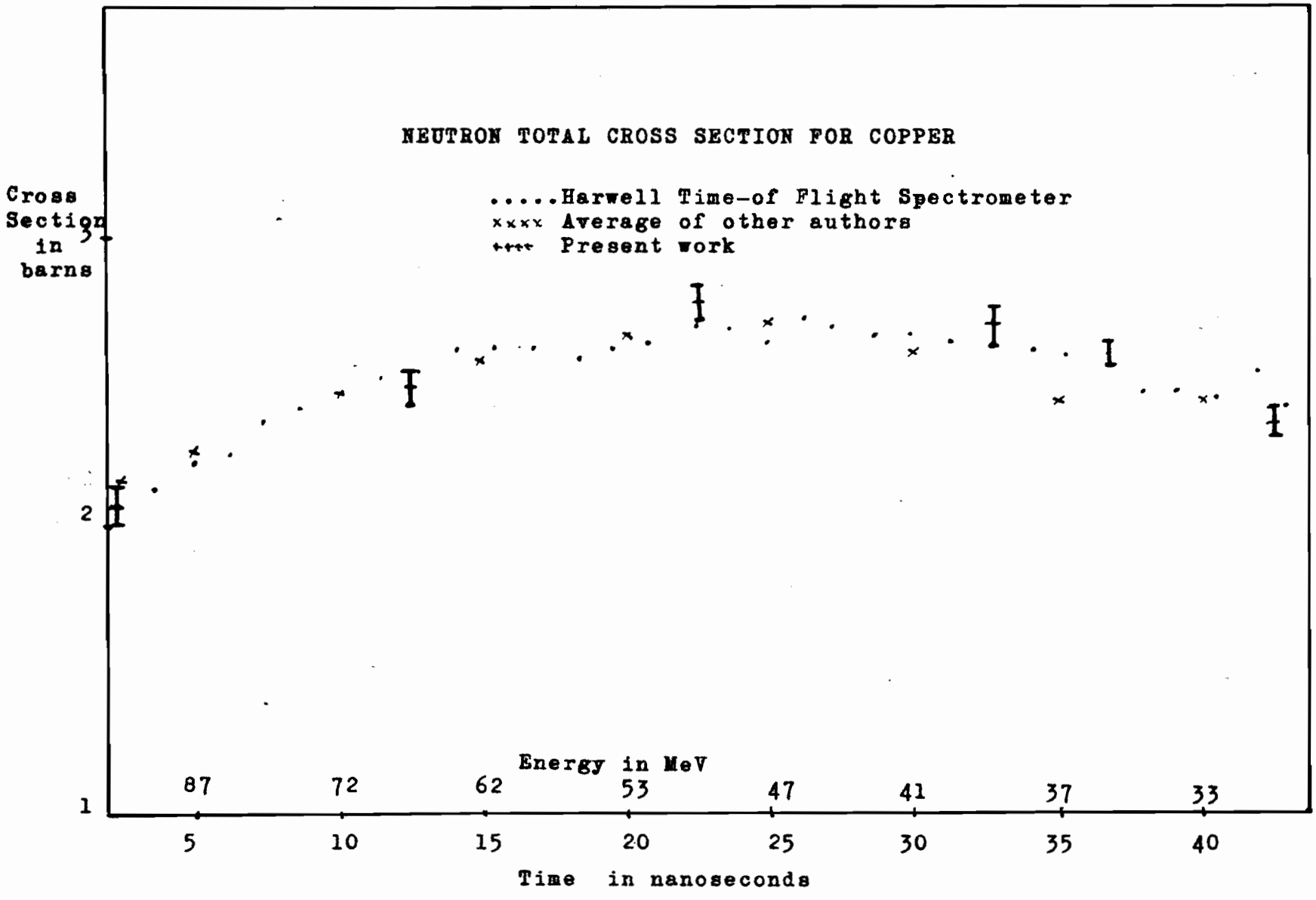
NEUTRON TOTAL CROSS SECTION FOR COPPER
.....Harwell Time-of Flight Spectrometer
×××× Average of other authors
++++ Present work
Cross Section in barns
3
2
1
Energy in MeV
87
72
62
53
47
41
37
33
5
10
15
20
25
30
35
40
Time in nanoseconds

FIG 17

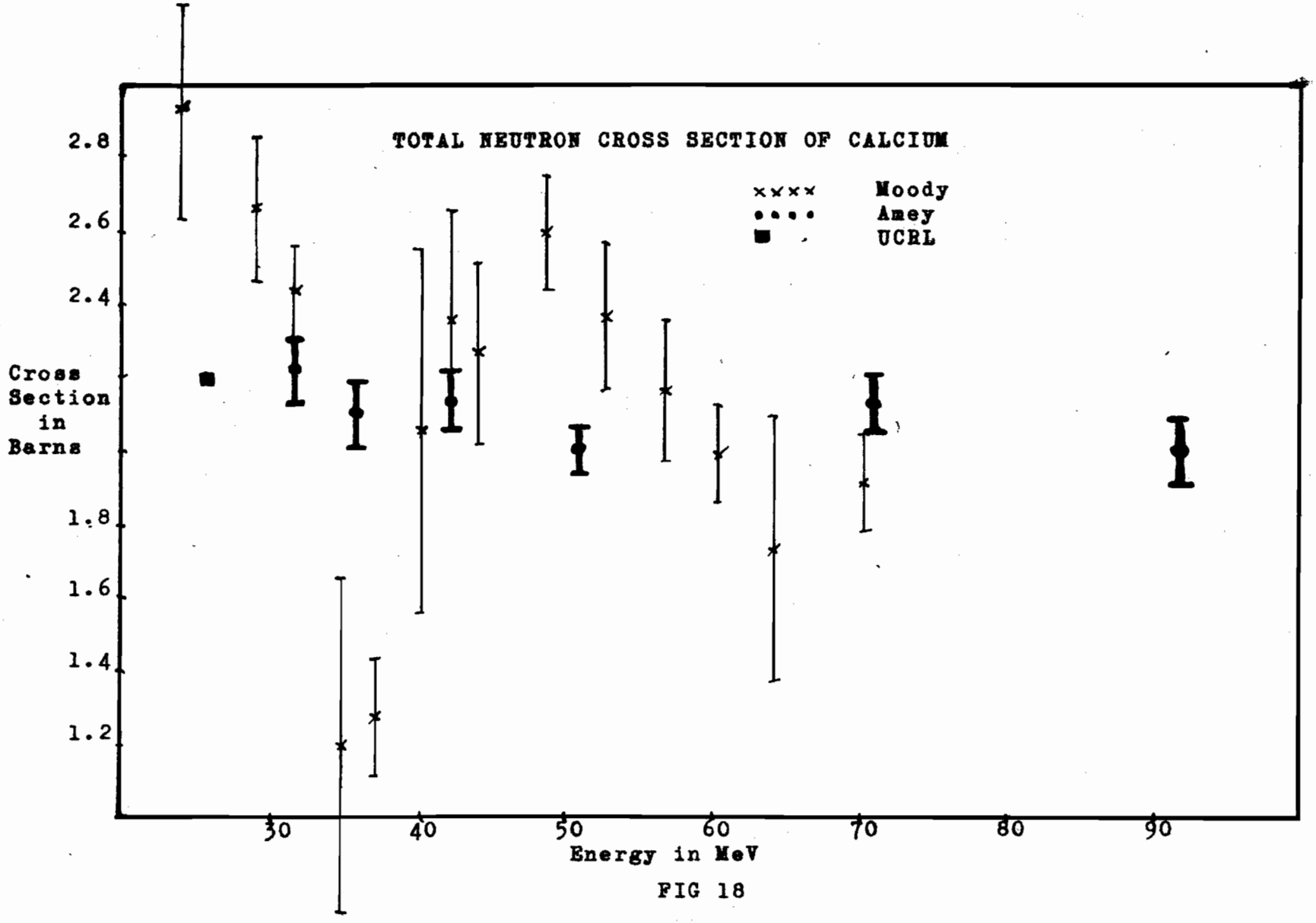
TOTAL NEUTRON CROSS SECTION OF CALCIUM
Moody
Amey
UCRL
Cross Section in Barns
2.8
2.6
2.4
1.8
1.6
1.4
1.2
30
40
50
60
70
80
90
Energy in MeV

FIG 18

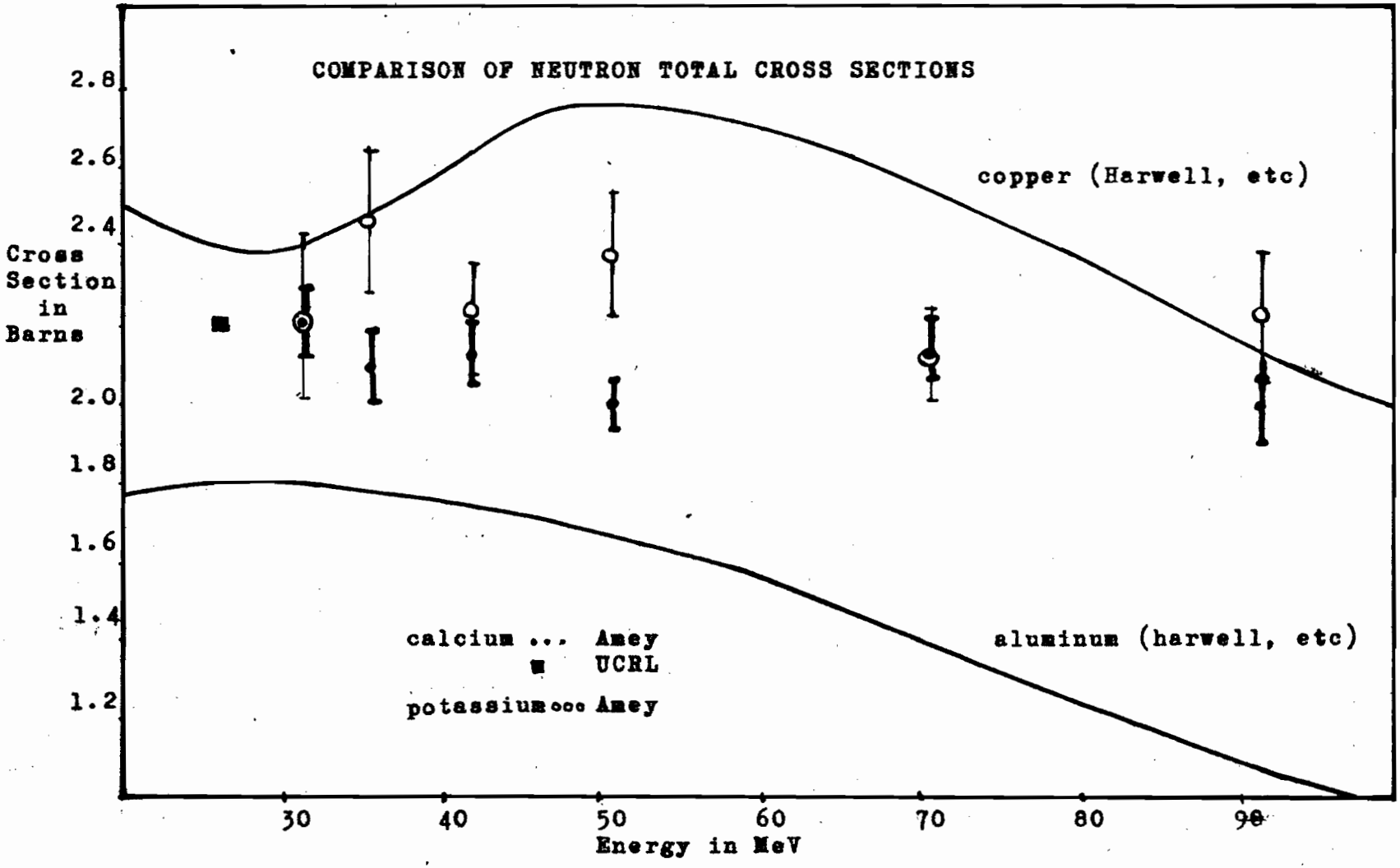
COMPARISON OF NEUTRON TOTAL CROSS SECTIONS
Cross Section in Barns
2.8
2.6
2.4
2.0
1.8
1.6
1.4
1.2
copper (Harwell, etc)
aluminum (harwell, etc)
calcium ... Amey
UCRL
potassium ooo Amey
30
40
50
60
70
80
90
Energy in MeV

FIG 19

as seen in Fig. 17. The lengths of the absorbers were so chosen that they all gave an attenuation of about 2/3 so that counting-rate effects should be similar.

Energy (MeV)	Cross Section (barns) Calcium	Potassium
31.5	2.22 - .09	2.22 - .19
35.7	2.10 - .09	2.47 - .18
42.2	2.14 - .08	2.22 - .14
51.0	2.01 - .06	2.39 - .15
71.0	2.14 - .07	2.12 - .12
91.6	2.01 - .08	2.22 - .16

4.6 Discussion of Experimental Results

The results obtained for calcium are shown in Fig. 18 compared with those of Moody and UCRL. Because of the poor statistics in Moody's experiment, the error-bars on his points are very large. As a consequence, there is no real discrepancy between his and the present results, which do not show the large dip in the cross section near 36 MeV which his results appeared to indicate.

As seen the above table and in Fig. 19, there do not appear to be statistically significant differences between the cross sections for calcium and potassium, the points indicating a gradual decrease as energy increases, as is also the case with aluminum. Evidence for maxima and min-

ima would require a wider energy range than was here available.

5. CONCLUSION

A time-of-flight spectrometer having an intrinsic time resolution better than one nanosecond, has been constructed using novel circuitry based on avalanche transistors.

The time structure of proton bursts in the external beam of the McGill cyclotron was measured and found to vary between three and seven nanoseconds, at half maximum, as a function of operating conditions. By continuous monitoring of the proton beam it may be possible to maintain a time resolution of three nanoseconds.

The neutron total cross section was measured for calcium and potassium, the deep minimum found by Moody not being confirmed although the resolution was sufficient to indicate such a dip. The cross section obtained for copper agreed with the values obtained by other investigators.

An improvement suggested by Dr. R.E. Bell would certainly enhance the usefulness of such equipment.

He suggested that each alternate burst of proton pulses be swept aside before they impinge on the neutron generator, so that the unfortunate shortening of the useful time range associated with the present 46 nanosecond periodicity would be somewhat alleviated. The flight path should be lengthened to improve time resolution, however no very notable improvement can be achieved by this method. It would be preferable to move the path out of the cyclotron vault into an environment where background and collimation problems are not as severe as they are at present.

REFERENCES

1. J.P.Scanlon, G.H. Stafford, J.J. Thresher and P.H. Bowen, Rev. Sci. Inst. Vol. 28, 749-757 (1957)
2. R.C. Mobley, Phys. Rev. Vol. 88, 360-361 (1952)
3. H.E. Bethe, Phys. Rev. Vol. 47, 747 (1935)
4. H.H. Barschall, Phys. Rev. Vol. 86, 431 (1952)
5. H. Feshbach, C.E. Porter, and V.F. Weisskopf, Phys. Rev., Vol. 90, 166 (1953); Vol. 96, 448 (1954)
6. J.M. Peterson, Phys. Rev. Vol. 125, 955 (1962)
7. F. Bjorklund and S. Fernbach, Phys. Rev. Vol. 109, 1295 (1958)
8. W.B. Riesenfeld and K.M. Watson, Phys. Rev. Vol. 102, 1157 (1956)
9. R.E. Bell, R.L. Graham and H.E. Petch, Can. J. of Phys. Vol. 30, 35 (1952)
10. C.E. Wiegand, T. Elioff, W.B. Johnson, L.B. Auerbach, J. Lach and T. Ypsilantis, Rev. Sci. Inst. Vol. 33, 526, (1962)

11. H.J. Moody, Ph.D. Thesis, McGill University, 1955

12. J.A. Hoffmann and K. Strauch, Phys. Rev. Vol. 90, 449 (1953)

13. J.L. Moll and R. Shen, Proc. I.R.E., Vol. 50, 43 (1962)

14. J.C. Hardy, M.Sc. Thesis, McGill University, 1963

15. P.H. Bowen, J.P. Scanlon, G.H. Stafford, and J.J. Thresher, Nuc. Phys., Vol. 22, 640 (1961)

16. D.W. Miller, Fast Neutron Physics Pt. II, 1000 (Interscience)